Ritz solution for transient analysis of variable stiffness shell structures

Giuseppe Sciascia*
University of Palermo, 90128, Palermo, Italy

Vincenzo Oliveri†
University of Limerick, Limerick V94-T9PX, Ireland

Alberto Milazzo‡
University of Palermo, 90128, Palermo, Italy

Paul M. Weaver§
University of Limerick, Limerick V94-T9PX, Ireland

The dynamic response of thin-walled structures is driven by mass and stiffness distribution. As such, variable stiffness composites offer opportunities to tune structural dynamic responses. To this extent, efficient analysis tools become increasingly important for structural analysis and design purposes. In this work, an efficient and versatile Ritz method for free vibrations and linear transient analysis of variable stiffness doubly-curved shell structures is presented. Variable stiffness shell structures are modeled as an assembly of shell-like domains. The shell kinematics are based on first-order shear deformation theory and no further assumption is made on the shallowness or on the thinness of the structure. The description of the shell is provided by a rational Bézier surface representation and general surface geometries can be represented. Legendre polynomials are employed to approximate the displacement field and penalty techniques are used to enforce displacement continuity and kinematical boundary conditions. Classical Rayleigh damping is considered and solutions are obtained through the Newmark integration. The resulting model allows a wide range of configurations and load cases for multi-component, variable stiffness composite structures to be solved, providing the same levels of accuracy as finite element analysis yet with a reduced number of variables and simpler data preparation.

*M.Eng. student, Dipartimento di Ingegneria, Vialed delle Scienze, Building 8, AIAA Student Member.
†School of Engineering and Bernal Institute, AIAA Member (Corresponding Author).
‡Professor, Dipartimento di Ingegneria, Vialed delle Scienze, Building 8, AIAA Senior Member.
§Professor and Bernal Chair, School of Engineering and Bernal Institute, AIAA Associate Member.

Nomenclature

$\mathcal{R}(x_1, x_2, x_3)$	=	global cartesian coordinate system
$\widetilde{\mathcal{R}}(\xi_1, \xi_2, \tilde{\zeta})$	=	local curvilinear reference system
$\boldsymbol{\Lambda}$	=	transformation matrices from the local to the global reference systems
$\boldsymbol{r}$	=	position vector of a point on the shell's reference surface
$\bar{\zeta}$	=	offset of the shell's mid-surface
$\boldsymbol{g}_1, \boldsymbol{g}_2$	=	tangent vectors along the ξ_1 and ξ_2 lines
a_1, a_2	=	metrics of surface first fundamental form
$\hat{\boldsymbol{n}}$	=	unit vector normal to the reference surface
L, N	=	metrics of surface second fundamental form
k_1, k_2	=	principal curvatures of the shell
R_1, R_2	=	principal radii of curvature of the shell
Ω	=	shell reference plane
$\partial\Omega$	=	boundary of the shell reference plane
$\partial\Omega_c, \partial\Omega_l$	=	kinematically constrained and loaded part of shell boundary
Γ_{pq}	=	common edge between pth and qth shells
$x_{\alpha_{i,j}}$	=	coordinates of the Bézier net control points
$\boldsymbol{d}, \dot{\boldsymbol{d}}$	=	displacement vector and its first time derivative
d_1, d_2, d_3	=	displacement components
u_1, u_2, u_3	=	translational displacement of the shell reference surface
$\vartheta_1, \vartheta_2, \vartheta_3$	=	rotational displacement of the shell reference surface
e_{ij}	=	strain components
$\boldsymbol{e}_p, \boldsymbol{e}_n$	=	in-plane and out-of-plane strain vectors
$\boldsymbol{\varepsilon}, \boldsymbol{\kappa}, \boldsymbol{\gamma}$	=	generalized strains, shell curvatures, and generalized shear strains vectors
$\boldsymbol{\mathscr{Z}}_L, \boldsymbol{\mathscr{Z}}_S$	=	shell curvature operator matrices
$\boldsymbol{\mathscr{D}}_p, \boldsymbol{\mathscr{D}}_n$	=	in-plane and out-of-plane differential operators
$\boldsymbol{\sigma}_p, \boldsymbol{\sigma}_n$	=	in-plane and out-of-plane stress vectors
$\theta(x_1, x_2)$	=	laminate fiber angle
$\boldsymbol{Q_p}, \boldsymbol{Q_n}$	=	in-plane and out-of-plane stiffness matrices
K	=	shell kinetic energy
U	=	shell internal energy
V_e	=	work of external forces

V_d	=	work of dissipative forces
$\boldsymbol{I_0}, \boldsymbol{I_1}, \boldsymbol{I_2}$	=	inertia matrices
$\boldsymbol{A}, \boldsymbol{B}, \boldsymbol{D}, \boldsymbol{A}_S$	=	laminate stiffness matrices
K_S	=	shear correction factor
$\boldsymbol{N}, \boldsymbol{M}, \boldsymbol{T}$	=	generalized stresses, moments and shear forces
$\boldsymbol{\Xi}$	=	Boolean matrix operator
$\bar{\boldsymbol{u}}, \bar{\boldsymbol{\vartheta}}$	=	prescribed generalized displacements and rotations
$\boldsymbol{q}, \boldsymbol{m}$	=	forces and moments per unit area applied on the shell domain
$\widetilde{\boldsymbol{N}}, \bar{\boldsymbol{N}}$	=	resultant forces applied on the shell's boundary
$\widetilde{\boldsymbol{M}}, \bar{\boldsymbol{M}}$	=	resultant moments applied on the shell's boundary
R_d	=	Rayleigh dissipation
$\boldsymbol{C}$	=	Rayleigh damping coefficients matrix
$\boldsymbol{C_0}, \boldsymbol{C_1}, \boldsymbol{C_2}$	=	Rayleigh damping matrices
$\zeta_{i,j}$	=	Rayleigh damping factors
$\boldsymbol{\omega}$	=	matrices of penalty coefficients
$\psi_i(\xi_1, \xi_2)$	=	trial functions
$\boldsymbol{\Psi}$	=	vectors of trial functions
$\boldsymbol{\Phi}$	=	matrix of trial functions
$\boldsymbol{\mathcal{B}}_p, \boldsymbol{\mathcal{B}}_n$	=	in-plane and out-of-plane discrete differential operators
$\boldsymbol{C}_\tau$	=	vectors of Ritz coefficients
$\boldsymbol{U}, \dot{\boldsymbol{U}}, \ddot{\boldsymbol{U}}$	=	vector of Ritz coefficients of displacement trial functions and its time derivatives
$\boldsymbol{\Theta}, \dot{\boldsymbol{\Theta}}, \ddot{\boldsymbol{\Theta}}$	=	vector of Ritz coefficients of rotation trial functions and its time derivatives
$\boldsymbol{X}, \dot{\boldsymbol{X}}, \ddot{\boldsymbol{X}},$	=	vectors collecting Ritz coefficients and its time derivatives
$\boldsymbol{K}_M$	=	system mass matrix
$\boldsymbol{K}_C$	=	system damping matrix
$\boldsymbol{K}_0$	=	system stiffness matrix
$\boldsymbol{R}$	=	system penalty matrices for shell boundary conditions
$\boldsymbol{P}_{pq}$	=	system penalty matrices for shell continuity conditions
$\boldsymbol{F}_D, \boldsymbol{F}_L$	=	system domain and boundary loads vectors
R_P	=	number of polynomials used for displacement approximation
R_D	=	number of domains used in structure's decomposition

Superscripts

$\bullet^{\langle k \rangle}$ = notation for quantities of kth shell domain

Subscripts

$\bullet_{\boldsymbol{u}}$ = notation for translational displacement related quantities

$\bullet_{\boldsymbol{\vartheta}}$ = notation for rotational displacement related quantities

I. Introduction

By virtue of their high stiffness and strength-to-weight ratios, thin walled composite shell structures are common essential components of advanced aerospace, naval and automotive engineering structures. Furthermore, the introduction of variable stiffness composites [1, 2] gave the designer a new way of tailoring the performance of laminated composites by changing the lamination angle at the ply level within the planform of the structure. It is well established that variable stiffness (VS) laminates can improve the buckling [3–5] structural response allowing additional weight reduction to be achieved when compared to straight fiber laminates. On the other hand, the primary load carrying structures in aerospace and automotive applications are subjected to dynamic loads under different operating conditions. These structures when subjected to time-periodic loads can undergo resonance for certain combinations of excitation frequency and amplitude of the applied load. Therefore, understanding the dynamic response characteristics of high performance lightweight structures is important from both a theoretical and design point of view. This aspect becomes even more important when considering VS laminates, as the fiber angle variation of the laminate can also be used to improve the dynamic response by tailoring the structural stiffness [6], even though it implicitly causes a more complex vibration response of the structure when it undergoes time-dependent loadings. The importance of these aspects is supported by the presence of extensive literature devoted to the study of the dynamic response of VS plates and shells. Referring to the analysis of plates within the finite element (FE) framework, Ribeiro and Akhavan[7] used a p-version FE formulation to carry out the free vibration and transient analysis of VS composite plates using a first order shear deformation theory and taking geometric non-linearity into account. Also, a p-version FE with a third-order shear deformation theory description has been used by Akhavan and Ribeiro [8] to study the linear free vibration of VS composite plates. The same framework has been used later by Ribeiro and Yazdani [9] to perform linear free vibration analysis of thick composite laminates with curvilinear fibres using a layerwise description. Ribeiro and Akhavan also presented a FE approach along with a shooting method to find periodic solutions of the equations of motion [10] and to study the non-linear forced vibration problem of imperfect VS laminated plates [11]. More complex and specific case studies have been also considered; Guenanou and Houmat [12] studied the free vibrations of symmetrically laminated VS composite circular plates using hierarchical finite elements with first order shear deformation theory (FSDT). More recently, Houmat [13] applied the p-version of the finite element method for the three-dimensional free vibration analysis

of VS plates. Samukham et al. [14] developed a FE analysis tool to study the dynamic instability of simply supported VS composite plates with delamination around a cutout in the framework of the FSDT theory. Zhao and Kapania [6] implemented a FE approach to study the vibration modes of a prestressed stiffened VS composite plate.

As an alternative to FE solutions for plate problems, Vescovini and Dozio [15] applied the variable-kinematic Ritz approach within Carrera's unified formulation (CUF) framework to study free vibrations of VS laminated plates. Tan and Nie [16] studied the free and forced vibration problem of annular thin VS composite plates with elastically restrained edges by the method of weighted residuals. Akbarzadeh et al. [17] used a hybrid Fourier-Galerkin method with third-order shear deformation theory to retrieve the forced vibration response of moderately-thick VS composite plates. Heydarpour and Aghdam [18, 19] presented transient analysis of VS composite plates in the framework of three dimensional theory of elasticity implementing a layer-wise differential quadrature method (DQM) and a mixed integral–differential quadrature method developing a new multi-step time integration method.

Focussing attention on the FE analysis of VS composite shells, FE solutions have been presented by Lo and Hyer [20] for free vibration of thin-walled elliptical VS composite cylinders. Ribeiro and Stoykov [21, 22] implemented the p-version finite element approach for the geometrically nonlinear free and forced vibration response of thin cylindrical VS composite shells.

In the framework of generalised differential quadrature method (GDQM), solutions for the free vibration analysis of VS composites conical shells treated by the FSDT theory have been presented by Wu and Lee [23]. Tornabene et al. [24] applied the Local Generalized Differential Quadrature (LGDQ) in the Carrera Unified Formulation (CUF) framework for the free vibration analysis of singly and doubly-curved VS panels. Recently, Tornabene et al. used the LGDQ method along with the CUF formulation to solve the free vibration problem of doubly-curved sandwich shells[25]. Samukham et al. [26] presented GDQM solutions of the dynamic instability problem of VS composite thin shallow shells. Venkatachari et al. [27] studied the free vibration characteristics of VS cylindrical and spherical composite shells using of a higher-order structural theory with a Galerkin framework.

Despite many works discussing the linear and nonlinear dynamic analysis of VS shells, the literature survey shows that most of the published works are limited to shells of revolution. With particular reference to the dynamic response of VS shell structures, to the best of the authors' knowledge no damping has been considered in previous works. Furthermore, mesh-based approaches, when applied to VS laminates, often require a discretization of the fiber angle variation as an element-wise constant value, making the solution even more mesh-size dependent whilst requiring ad-hoc mesh data preparation routines. This aspect makes mesh-less techniques appealing, since in such methods no further approximations need to be introduced to model VS composite layups and the fiber angle variation can be expressed as a continuous function within the integration domain. Among various mesh-less approaches, the Ritz method has been successfully applied to many static and dynamic problems. Gulizzi et al. and Oliveri et al. applied the Ritz method for the linear buckling and geometrically nonlinear analyses of VS composite structures [28–30], showing its accuracy and

computational efficiency when compared to FE solutions. Focussing on Ritz solutions for the dynamic behaviour of VS laminated composites, only two works have so far been proposed, Chen et al. [31] and Loja et al. [32], showing the method's potential robustness, even though their solutions are limited to flat plate configurations.

With these limitations in mind, the aim of this work is to develop an efficient Ritz analysis tool for the free vibration and the linear transient analysis of variable stiffness doubly-curved laminated shell structures undergoing arbitrary loads and boundary conditions. The shell model is based on first-order shear deformation theory and no further assumption is made on the shallowness or on the thinness of the structure. General stacking sequences are considered and Legendre orthogonal polynomials are employed to approximate the unknown displacement field. Stiffened variable angle tow shell structures are modeled as an assembly of shell-like domains and penalty techniques are used to enforce the displacement continuity of the assembled multi-domain structure and kinematical boundary conditions. For the forced vibration response, classical Rayleigh damping is considered and solutions are obtained through the Newmark integration scheme [33]. This approach has: (i) the advantage of simple preprocessing, as it only requires the geometrical information of the shell and the function that analytically describes the fiber variation within the composite layup; (ii) the feature to capture the geometrical description of the shell structure through a rational Bézier surface representation so that no geometrical approximation is introduced; (iii) the versatility to model a wide range of configurations and load cases for multi-component, variable stiffness composite structures, providing the same levels of accuracy as finite element analysis with a reduced number of variables. The proposed solution is validated by comparison with literature and finite elements analyses and original results are presented for the free vibration and linear transient solution of VS stiffened shell structures showing the capability of the present method in modelling typical aerospace structural components such as curved stiffened panels and nacelles.

The work is organised as follow: the geometrical description and the shell formulation is presented in Sec.II. Next, details of the Ritz approximation procedure and the solution method are provided in Sec.III. Details of the model are presented in Sec.IV. The validation of the proposed method and original results are discussed in Sec.V, followed by concluding remarks in Sec.VI.

II. Formulation

The proposed modeling strategy relies on a decomposition of the entire structure into shell-like domains. In turn, the entire thin-walled structure is assembled by enforcing the boundary conditions for each component; these are given by displacement continuity and traction equilibrium along the edges joining different domains and by the external load and kinematical constraint conditions. These constraints are introduced with a penalty approach in a similar fashion to other works presented in the literature to assemble Ritz domains [34–37] and has been extended by the authors to account for an FSDT description with six degrees of freedom [28–30]. Note that within this work the decomposition of the structure into multiple domains has the sole purpose of enabling the modeling of complex multi-component

structures and the present Ritz approach relies on the number of polynomial trial functions used in the approximation of the displacement field in order to improve accuracy of the results (see Sec. III).

Consider a thin-walled structure treated as an assembly of R_D quadrilateral composite multilayered shells, as shown in Fig.1. Let the superscript k inside angle bracket denote quantities associated with the k-th domain. Each shell is an

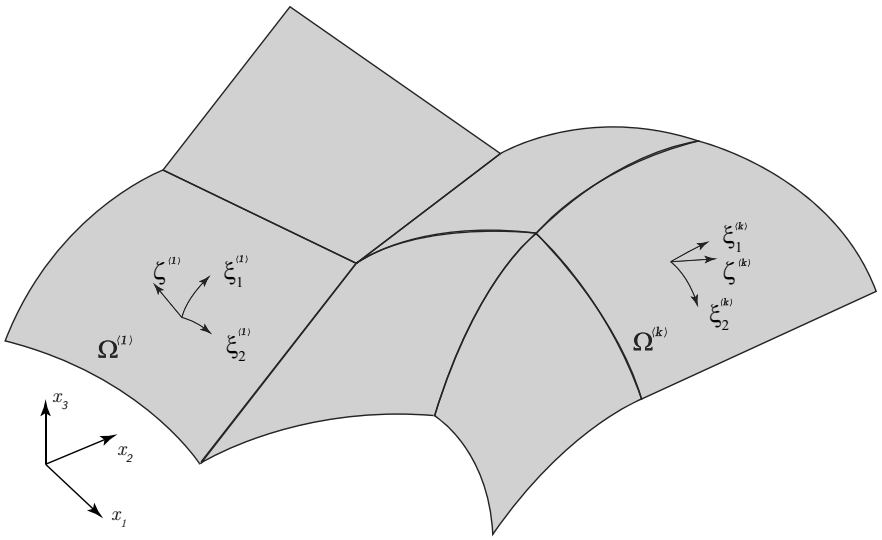

Figure 1 Assembled structure reference systems

N-layered quadrilateral domain with thickness h. Let us assume the layers have constant thickness and are made of homogeneous and orthotropic material. The shell can be kinematically constrained on the lateral boundary and it is subjected to domain and boundary loads as specified in the following Sections. The whole structure is referred to a global cartesian coordinate system $\mathcal{R}$ whose axes are denoted by x_i.

A. Shell's surface mapping

Consider the k-th shell of the thin-walled structure as an isolated structural entity. In this subsection, the superscript $\langle k\rangle$ is omitted to simplify visual complexity, but is restored later when relevant for the formulation development. Let the domain occupied by the shell reference plane be denoted by Ω with $\partial\Omega$ as its boundary. A uniform thickness curved shell domain is shown in Fig.2a, where $(\xi_1, \xi_2, \tilde{\zeta})$ denote the curvilinear coordinates spanning the reference surface ($\tilde{\zeta} = 0$). The position vector of a point $(\xi_1, \xi_2, 0)$ on the reference surface is denoted by $\boldsymbol{r}$. The mapping of the shell domain to the square domain $[-1, 1] \times [-1, 1]$ where integration rules are applied is done introducing a rational Bézier surface representation [38] . The components of the position vector $\boldsymbol{r}$ of the shell's reference plane are expressed as

$$r_\alpha = \sum_{i=0}^{n} \sum_{j=0}^{m} S_{i,j}(\xi_1, \xi_2)\, x_{\alpha_{i,j}} \qquad \alpha = 1,\ 2,\ 3 \tag{1}$$

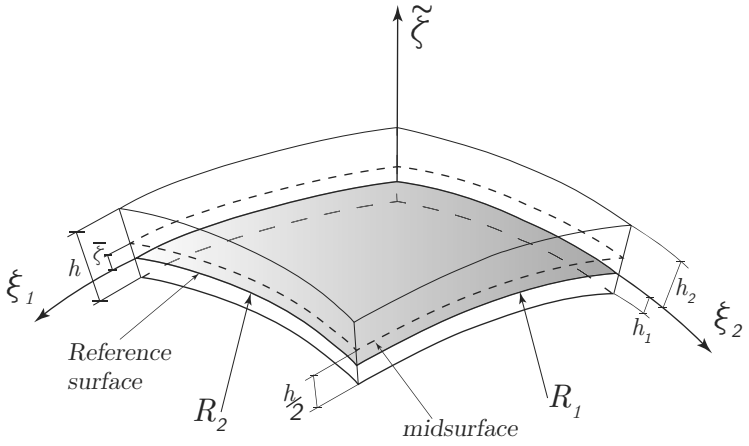

(a)

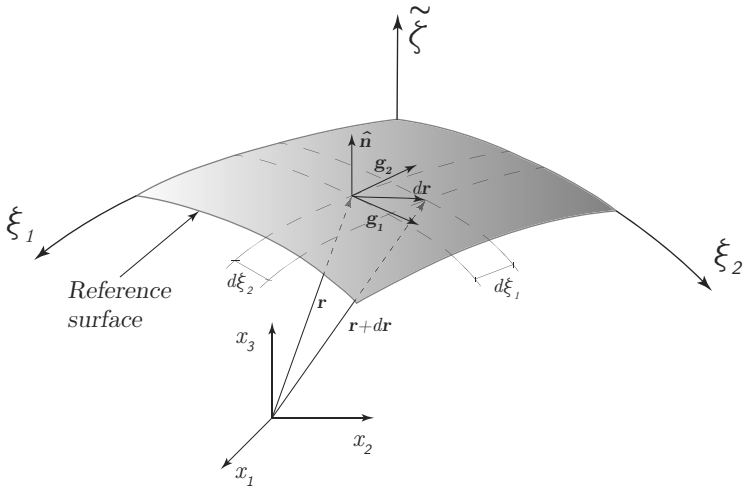

(b)

Figure 2 Shell domain geometry

where $x_{\alpha_{i,j}}$ are the coordinates of the Bézier net control points and

$$S_{i,j}(\xi_1,\xi_2) = \frac{B_{i,n}(\xi_1)\, B_{j,m}(\xi_2)\, w_{i,j}}{\sum_{r=0}^{n}\sum_{s=0}^{m} B_{r,n}(\xi_1)\, B_{s,m}(\xi_2)\, w_{r,s}}; \qquad \begin{cases} -1 \le \xi_1 \le 1 \\ -1 \le \xi_2 \le 1 \end{cases} \tag{2}$$

In Eq.(2), $B_{p,q}(\xi_k)$ are univariate Bernstein polynomials and $w_{p,q}$ are the control weights. Hence, the position vector $\boldsymbol{r}$ of a point $(\xi_1, \xi_2, 0)$ on the reference surface is expressed in compact matrix form as

$$\boldsymbol{r} = (\boldsymbol{S}(\xi_1,\xi_2)\boldsymbol{X})^T \tag{3}$$

where $\boldsymbol{X}$ is a $(n+1)(m+1)\times 3$ matrix that collect the coordinates $x_{\alpha_{i,j}}$ of the control points and $\boldsymbol{S}$ is a $1\times(n+1)(m+1)$ vector that collect the functions $S_{i,j}$. By differentiating Eq.(3) with respect to the ξ_1 and ξ_2 coordinates it becomes possible to obtain the vectors $\boldsymbol{g}_1$ and $\boldsymbol{g}_2$ tangent to the ξ_1 and ξ_2 lines and retrieve the first fundamental form quantities defined as

$$a_1^2 = \boldsymbol{g}_1 \cdot \boldsymbol{g}_1 \quad a_2^2 = \boldsymbol{g}_2 \cdot \boldsymbol{g}_2 \quad a_1 a_2\, cos\phi = \boldsymbol{g}_1 \cdot \boldsymbol{g}_2 \tag{4}$$

From this point forward, we assume that ξ_1 and ξ_2 are orthogonal such that ξ_1 and ξ_2 curves are the lines of principal curvature on the reference surface. Then

$$cos\phi = \frac{\boldsymbol{g}_1 \cdot \boldsymbol{g}_2}{a_1 a_2} = 0 \tag{5}$$

Note that as Eq.(3) is a general parametric description of a surface that maps the shell domain into a unit square, the orthogonality condition of the ξ_1 and ξ_2 coordinate lines, namely Eq.(5) has to be assessed in order to ensure that ξ_1 and ξ_2 curves are the lines of principal curvature on the reference surface. The unit normal vector to the reference surface $\hat{\boldsymbol{n}}$ can be determined as

$$\hat{\boldsymbol{n}} = \frac{\boldsymbol{g}_1 \times \boldsymbol{g}_2}{a_1 a_2} \tag{6}$$

Finally, considering the definition of the coefficients L and N of the second quadratic form of the reference surface [39], namely

$$L = \hat{\boldsymbol{n}} \cdot \frac{\partial^2 \boldsymbol{r}}{\partial {\xi_1}^2} \tag{7a}$$

$$N = \hat{\boldsymbol{n}} \cdot \frac{\partial^2 \boldsymbol{r}}{\partial {\xi_2}^2} \tag{7b}$$

and using Eq.(3), the curvatures k_1 and k_2 of the ξ_1 and ξ_2 lines can be evaluated as

$$k_1 = -\frac{L}{{a_1}^2} \tag{8a}$$

$$k_2 = -\frac{N}{{a_2}^2} \tag{8b}$$

B. First order kinematics

The first order shear deformation theory (FSDT) is considered and thus the displacement field referred to the $\widetilde{\mathcal{R}}(\xi_1, \xi_2, \tilde{\zeta})$ coordinate system is given by

$$d_1 = u_1(\xi_1, \xi_2, t) + (\zeta + \bar{\zeta})\vartheta_1(\xi_1, \xi_2, t) \tag{9a}$$

$$d_2 = u_2(\xi_1, \xi_2, t) + (\zeta + \bar{\zeta})\vartheta_2(\xi_1, \xi_2, t) \tag{9b}$$

$$d_3 = u_3(\xi_1, \xi_2, t) \tag{9c}$$

In Eq.(9), $\bar{\zeta}$ is the offset of the shell's mid-surface ($\zeta = 0$) with respect to the reference surface ($\zeta = -\bar{\zeta}$). Hence, u_1, u_2 are the displacement components of the points of the reference surface along the ξ_1 and ξ_2 axis, u_3 is the transverse deflection along the ζ direction, ϑ_1 and ϑ_2 are rotations of the transverse normal around the ξ_2 and ξ_1-axis, respectively. Eqs. (9) can be compactly written as

$$\boldsymbol{d} = \boldsymbol{u} + (\zeta + \bar{\zeta})\mathcal{L}\boldsymbol{\vartheta} \tag{10}$$

where $\boldsymbol{u}^T = \{u_1, u_2, u_3\}^T$, $\boldsymbol{\vartheta}^T = \{\vartheta_1, \vartheta_2, \vartheta_3\}^T$ and

$$\mathcal{L} = \begin{bmatrix} 1 & 0 & 0 \\ 0 & 1 & 0 \\ 0 & 0 & 0 \end{bmatrix} \tag{11}$$

Note that with the definition of the matrix $\mathcal{L}$ the introduction of the "drilling" rotation $\vartheta_3 = \vartheta_3(\xi_1, \xi_2)$ does not affect the displacement field. In the framework of small deflections and rotations, the strain-displacement relations [39] can be written in terms of generalized strains as

$$\boldsymbol{e}_p = \begin{Bmatrix} e_{11} \\ e_{22} \\ e_{12} \end{Bmatrix} = \boldsymbol{\mathcal{Z}}_L \left[\boldsymbol{\varepsilon} + (\zeta + \bar{\zeta})\boldsymbol{\kappa}\right] \tag{12a}$$

$$\boldsymbol{e}_n = \begin{Bmatrix} e_{13} \\ e_{23} \end{Bmatrix} = \boldsymbol{\mathcal{Z}}_S \boldsymbol{\gamma} \tag{12b}$$

where the matrices $\boldsymbol{\mathcal{Z}}_L$, $\boldsymbol{\mathcal{Z}}_S$ and the generalized strains are defined as

$$\boldsymbol{\mathcal{Z}}_L = \begin{bmatrix} \frac{1}{[1+k_1(\zeta+\bar{\zeta})]} & 0 & 0 & 0 \\ 0 & \frac{1}{[1+k_2(\zeta+\bar{\zeta})]} & 0 & 0 \\ 0 & 0 & \frac{1}{[1+k_1(\zeta+\bar{\zeta})]} & \frac{1}{[1+k_2(\zeta+\bar{\zeta})]} \end{bmatrix} \tag{13a}$$

$$\boldsymbol{\mathcal{Z}}_S = \begin{bmatrix} \frac{1}{[1+k_1(\zeta+\bar{\zeta})]} & 0 & 0 \\ 0 & \frac{1}{[1+k_2(\zeta+\bar{\zeta})]} & 0 \end{bmatrix} \tag{13b}$$

$$\boldsymbol{\varepsilon} = \begin{Bmatrix} \varepsilon_{11} \\ \varepsilon_{22} \\ \varepsilon_{12} \\ \varepsilon_{21} \end{Bmatrix} = \begin{bmatrix} \frac{1}{a_1}\frac{\partial}{\partial\xi_1} & \frac{1}{a_1 a_2}\frac{\partial a_1}{\partial\xi_2} & k_1 \\ \frac{1}{a_1 a_2}\frac{\partial a_2}{\partial\xi_1} & \frac{1}{a_2}\frac{\partial}{\partial\xi_2} & k_2 \\ -\frac{1}{a_1 a_2}\frac{\partial a_1}{\partial\xi_2} & \frac{1}{a_1}\frac{\partial}{\partial\xi_1} & 0 \\ \frac{1}{a_2}\frac{\partial}{\partial\xi_2} & -\frac{1}{a_1 a_2}\frac{\partial a_2}{\partial\xi_1} & 0 \end{bmatrix} \begin{Bmatrix} u_1 \\ u_2 \\ u_3 \end{Bmatrix} = \boldsymbol{\mathcal{D}}_{p\,u}\boldsymbol{u} \tag{14a}$$

$$\boldsymbol{\kappa} = \begin{Bmatrix} \kappa_{11} \\ \kappa_{22} \\ \kappa_{12} \\ \kappa_{21} \end{Bmatrix} = \begin{bmatrix} \frac{1}{a_1}\frac{\partial}{\partial\xi_1} & \frac{1}{a_1 a_2}\frac{\partial a_1}{\partial\xi_2} & 0 \\ \frac{1}{a_1 a_2}\frac{\partial a_2}{\partial\xi_1} & \frac{1}{a_2}\frac{\partial}{\partial\xi_2} & 0 \\ -\frac{1}{a_1 a_2}\frac{\partial a_1}{\partial\xi_2} & \frac{1}{a_1}\frac{\partial}{\partial\xi_1} & 0 \\ \frac{1}{a_2}\frac{\partial}{\partial\xi_2} & -\frac{1}{a_1 a_2}\frac{\partial a_2}{\partial\xi_1} & 0 \end{bmatrix} \begin{Bmatrix} \vartheta_1 \\ \vartheta_2 \\ \vartheta_3 \end{Bmatrix} = \boldsymbol{\mathcal{D}}_{p\,\vartheta}\boldsymbol{\vartheta} \tag{14b}$$

$$\boldsymbol{\gamma} = \begin{Bmatrix} \gamma_{13} \\ \gamma_{23} \\ 0 \end{Bmatrix} = \begin{bmatrix} -k_1 & 0 & \frac{1}{a_1}\frac{\partial}{\partial\xi_1} \\ 0 & -k_2 & \frac{1}{a_2}\frac{\partial}{\partial\xi_2} \\ 0 & 0 & 0 \end{bmatrix} \begin{Bmatrix} u_1 \\ u_2 \\ u_3 \end{Bmatrix} + \begin{bmatrix} 1 & 0 & 0 \\ 0 & 1 & 0 \\ 0 & 0 & 0 \end{bmatrix} \begin{Bmatrix} \vartheta_1 \\ \vartheta_2 \\ \vartheta_3 \end{Bmatrix} = \boldsymbol{\mathcal{D}}_{n\,u}\boldsymbol{u} + \boldsymbol{\mathcal{D}}_{n\,\theta}\boldsymbol{\vartheta} \tag{14c}$$

C. Shell Constitutive relations

Assuming plane stress conditions ($\sigma_{zz} = 0$), the elastic constitutive equations for the generally oriented $\kappa-$th orthotropic lamina, referred to the laminate coordinate system, are written as

$$\boldsymbol{\sigma}_p = \boldsymbol{Q}_p \boldsymbol{e}_p \tag{15a}$$

$$\boldsymbol{\sigma}_n = \boldsymbol{Q}_n \boldsymbol{e}_n \tag{15b}$$

Note that the (3×3) matrix $\boldsymbol{Q_p}$ and the (2×2) matrix $\boldsymbol{Q_n}$ that contain the ply stiffness coefficients depend on the fiber orientation θ of each ply. For VS composite shells they can be considered as a function of the in-plane coordinates of each layer being $\theta = \theta(\xi_1, \xi_2)$ [28].

D. Principle of Hamilton

The governing equations of the assembled structure are deduced through Hamilton's principle [40]. According to Rayleigh's damping approach [41], a separate functional is introduced to account for dissipative forces. Then, considering N_p domains, Hamilton's principle states that

$$\int_{t_1}^{t_2} \left\{ \sum_{k=1}^{R_D} \left[\delta \boldsymbol{K}^{\langle k \rangle} + (\delta \boldsymbol{U}^{\langle k \rangle} + \delta \boldsymbol{V_e}^{\langle k \rangle}) \right] \right\} dt - \int_{t_1}^{t_2} \left\{ \sum_{k=1}^{R_D} \delta \boldsymbol{V_d}^{\langle k \rangle} \right\} dt = 0 \tag{16}$$

where $K^{\langle k \rangle}$ is kinetic energy of the k-th shell, $U^{\langle k \rangle}$ is the strain energy, $V_e^{\langle k \rangle}$ and $V_d^{\langle k \rangle}$ are the works associated with external loads and dissipative forces respectively. In the following subsections the expressions of these energy quantities are derived.

1. Kinetic energy of the shell

First we observe that the infinitesimal volume element of the shell, considering the standard procedures of differential geometry, can be expressed as [39]

$$\begin{aligned} dV = &\left[1 + k_1(\zeta + \bar{\zeta})\right] \left[1 + k_2(\zeta + \bar{\zeta})\right] a_1 a_2 \, d\xi_1 d\xi_2 d\zeta = \\ &\left[1 + k_1(\zeta + \bar{\zeta})\right] \left[1 + k_2(\zeta + \bar{\zeta})\right] d\Omega d\zeta \end{aligned} \tag{17}$$

The kinetic energy of the shell can be written as

$$\begin{aligned} K = &\frac{1}{2} \int_V \dot{\boldsymbol{d}}^T \left(\boldsymbol{I}^3 \rho \right) \dot{\boldsymbol{d}} \, dV = \\ &\frac{1}{2} \int_\Omega \left[\left(\dot{\boldsymbol{u}}^T \boldsymbol{I_0} \dot{\boldsymbol{u}} \right) + \left(\dot{\boldsymbol{u}}^T \boldsymbol{I_1} \dot{\boldsymbol{\theta}} \right) + \left(\dot{\boldsymbol{\theta}}^T \boldsymbol{I_1}^T \dot{\boldsymbol{u}} \right) + \left(\dot{\boldsymbol{\theta}}^T \boldsymbol{I_2} \dot{\boldsymbol{\theta}} \right) \right] d\Omega \end{aligned} \tag{18}$$

where ρ is the density and $\boldsymbol{I}^3$ is a (3×3) identity matrix and $\dot{\boldsymbol{d}}$ is the temporal derivative of the displacement field, namely Eq.(10). The inertia matrices $\boldsymbol{I_0}, \boldsymbol{I_1}, \boldsymbol{I_2}$ are defined as

$$\begin{aligned} \boldsymbol{I_0} &= \int_\zeta \left(\boldsymbol{I}^3 \rho \right) \left[1 + k_1 \left(\zeta + \bar{\zeta}\right)\right] \left[1 + k_2 \left(\zeta + \bar{\zeta}\right)\right] d\zeta \\ \boldsymbol{I_1} &= \int_\zeta \left(\boldsymbol{I}^3 \rho \right) \mathcal{L} \left(\zeta + \bar{\zeta}\right) \left[1 + k_1 \left(\zeta + \bar{\zeta}\right)\right] \left[1 + k_2 \left(\zeta + \bar{\zeta}\right)\right] d\zeta \\ \boldsymbol{I_2} &= \int_\zeta \mathcal{L}^T \left(\boldsymbol{I}^3 \rho \right) \mathcal{L} \left(\zeta + \bar{\zeta}\right)^2 \left[1 + k_1 \left(\zeta + \bar{\zeta}\right)\right] \left[1 + k_2 \left(\zeta + \bar{\zeta}\right)\right] d\zeta \end{aligned} \tag{19}$$

2. Internal energy of the shell

The internal energy of the shell is written as

$$
\begin{aligned}
U =& \frac{1}{2}\int_V \left(\boldsymbol{e}_p^T\boldsymbol{\sigma}_p + \boldsymbol{e}_n^T\boldsymbol{\sigma}_n\right) dV = \\
& \frac{1}{2}\int_\Omega \sum_{k=1}^{N}\int_{h_{k-1}}^{h_k} \left(\boldsymbol{e}_p^T\boldsymbol{\sigma}_p + \boldsymbol{e}_n^T\boldsymbol{\sigma}_n\right)\left[1+k_1\left(\zeta+\bar{\zeta}\right)\right]\left[1+k_2\left(\zeta+\bar{\zeta}\right)\right] d\zeta\, d\Omega = \\
& \frac{1}{2}\int_\Omega \left[\boldsymbol{\varepsilon}^T\left(\boldsymbol{A}\boldsymbol{\varepsilon}+\boldsymbol{B}\boldsymbol{\kappa}\right) + \boldsymbol{\kappa}^T\left(\boldsymbol{B}\boldsymbol{\varepsilon}+\boldsymbol{D}\boldsymbol{\kappa}\right) + \boldsymbol{\gamma}^T\left(\boldsymbol{A}_S\boldsymbol{\gamma}\right)\right] d\Omega
\end{aligned}
\tag{20}
$$

In Eq.(20), resultant forces and moments acting over the shell's modeling plane have been defined as

$$
\boldsymbol{N} = \begin{Bmatrix} N_{11} \\ N_{22} \\ N_{12} \\ N_{21} \end{Bmatrix} = \int_{-h/2}^{h/2} \widetilde{\boldsymbol{\mathscr{Z}}}_L\, \boldsymbol{\sigma}_p\, d\zeta = \left[\sum_{k=1}^{n_p}\int_{h_{k-1}}^{h_k} \widetilde{\boldsymbol{\mathscr{Z}}}_L\, \boldsymbol{Q}_p\, \boldsymbol{\mathscr{Z}}_L\, d\zeta\right]\boldsymbol{\varepsilon} + \left[\sum_{k=1}^{n_p}\int_{h_{k-1}}^{h_k} \widetilde{\boldsymbol{\mathscr{Z}}}_L\, \boldsymbol{Q}_p\, \boldsymbol{\mathscr{Z}}_L\, (\zeta+\bar{\zeta})d\zeta\right]\boldsymbol{\kappa} = \boldsymbol{A}\boldsymbol{\varepsilon} + \boldsymbol{B}\boldsymbol{\kappa} \tag{21a}
$$

$$
\boldsymbol{M} = \begin{Bmatrix} M_{11} \\ M_{22} \\ M_{12} \\ M_{21} \end{Bmatrix} = \int_{-h/2}^{h/2} \widetilde{\boldsymbol{\mathscr{Z}}}_L\, \boldsymbol{\sigma}_p (\zeta+\bar{\zeta}) d\zeta = \left[\sum_{k=1}^{n_p}\int_{h_{k-1}}^{h_k} \widetilde{\boldsymbol{\mathscr{Z}}}_L\, \boldsymbol{Q}_p\, \boldsymbol{\mathscr{Z}}_L\, (\zeta+\bar{\zeta})d\zeta\right]\boldsymbol{\varepsilon} + \left[\sum_{k=1}^{n_p}\int_{h_{k-1}}^{h_k} \widetilde{\boldsymbol{\mathscr{Z}}}_L\, \boldsymbol{Q}_p\, \boldsymbol{\mathscr{Z}}_L\, (\zeta+\bar{\zeta})^2 d\zeta\right]\boldsymbol{\kappa} = \boldsymbol{B}\boldsymbol{\varepsilon} + \boldsymbol{D}\boldsymbol{\kappa} \tag{21b}
$$

$$
\boldsymbol{T} = \begin{Bmatrix} T_{13} \\ T_{23} \\ 0 \end{Bmatrix} = \int_{-h/2}^{h/2} K_S \widetilde{\boldsymbol{\mathscr{Z}}}_S\, \boldsymbol{\sigma}_n\, d\zeta = \left[\sum_{k=1}^{n_p}\int_{h_{k-1}}^{h_k} K_S \widetilde{\boldsymbol{\mathscr{Z}}}_S\, \boldsymbol{Q}_n\, \boldsymbol{\mathscr{Z}}_S\, d\zeta\right]\boldsymbol{\gamma} = \boldsymbol{A}_S\boldsymbol{\gamma} \tag{21c}
$$

where, $\widetilde{\boldsymbol{\mathscr{Z}}}_L = \left[1+k_1(\zeta+\bar{\zeta})\right]\left[1+k_2(\zeta+\bar{\zeta})\right]\boldsymbol{\mathscr{Z}}_L^T$ and $\widetilde{\boldsymbol{\mathscr{Z}}}_S = \left[1+k_1(\zeta+\bar{\zeta})\right]\left[1+k_2(\zeta+\bar{\zeta})\right]\boldsymbol{\mathscr{Z}}_S^T$. In Eqs.(21), n_p is the total number of plies within the laminate whereas h_{k-1} and h_{k-1} are the bottom and top face ζ coordinates of the k-th ply, respectively. Also, in Eq.(21c), the shear correction factor K_S has been introduced. Finally, Eqs.(21) can be compactly written as

$$
\begin{Bmatrix} \boldsymbol{N} \\ \boldsymbol{M} \\ \boldsymbol{T} \end{Bmatrix} = \begin{bmatrix} \boldsymbol{A} & \boldsymbol{B} & 0 \\ \boldsymbol{B} & \boldsymbol{D} & 0 \\ 0 & 0 & \boldsymbol{A}_S \end{bmatrix} \begin{Bmatrix} \boldsymbol{\varepsilon} \\ \boldsymbol{\kappa} \\ \boldsymbol{\gamma} \end{Bmatrix} \tag{22}
$$

3. Work done by shell's external forces

The work done by external loads acting on the shell is written as

$$\begin{aligned} V_e = &- \int_{\Omega} \left[\boldsymbol{u}^T \boldsymbol{q} + \boldsymbol{\vartheta}^T \boldsymbol{m} \right] d\Omega \\ &- \int_{\partial\Omega_l} \left[\boldsymbol{u}^T \bar{\boldsymbol{N}} + \boldsymbol{\vartheta}^T \bar{\boldsymbol{M}} \right] d\partial\Omega \\ &- \int_{\partial\Omega_c} \left[\boldsymbol{u}^T \widetilde{\boldsymbol{N}} + \boldsymbol{\vartheta}^T \widetilde{\boldsymbol{M}} \right] d\partial\Omega \end{aligned} \tag{23}$$

In Eq.23, the external loads and constraint reactions of the shell consist of the forces $\boldsymbol{q} = \{q_1 \ q_2 \ q_3\}^T$ and moments $\boldsymbol{m} = \{m_1 \ m_2 \ 0\}^T$ per unit area applied over the domain Ω and the resultant forces $\widetilde{\boldsymbol{N}} = \{\widetilde{N}_1 \ \widetilde{N}_2 \ \widetilde{N}_3\}^T$ and moments $\widetilde{\boldsymbol{M}} = \{\widetilde{M}_1 \ \widetilde{M}_2 \ 0\}^T$ per unit length applied on the boundary $\partial\Omega$. On the loaded part of the plate boundary $\partial\Omega_l$, is $\widetilde{\boldsymbol{N}} = \bar{\boldsymbol{N}}$ and $\widetilde{\boldsymbol{M}} = \bar{\boldsymbol{M}}$, where the overbar denotes prescribed quantities.

The essential boundary conditions of the shell are provided prescribing the generalized displacements on the part $\partial\Omega_c$ of the boundary and they read as

$$\boldsymbol{\Xi}_u \boldsymbol{u} = \boldsymbol{\Xi}_u \bar{\boldsymbol{u}} \quad \text{on } \partial\Omega_c \tag{24a}$$

$$\boldsymbol{\Xi}_\vartheta \boldsymbol{\vartheta} = \boldsymbol{\Xi}_\vartheta \bar{\boldsymbol{\vartheta}} \quad \text{on } \partial\Omega_c \tag{24b}$$

where, again, the overbar denotes prescribed quantities and $\boldsymbol{\Xi}_u$ and $\boldsymbol{\Xi}_\vartheta$ are suitable Boolean matrix operators that select the constrained components of the generalized displacements vectors. It should to be mentioned that both external loads and constraint reactions can depend on time.

4. Shell's viscous damping

Rayleigh's dissipation factor R_d can be defined as [42]

$$R_d = \frac{1}{2} \int_V \dot{\boldsymbol{d}}^T \boldsymbol{C} \dot{\boldsymbol{d}} \, dV \tag{25}$$

where $\boldsymbol{C}$ is the damping matrix. This expression allows the work done by dissipative forces, namely $\boldsymbol{V}_d$, to be written as:

$$\begin{aligned} V_d = \int_V \boldsymbol{d}^T \left(\frac{\partial R_d}{\partial \dot{\boldsymbol{d}}} \right) dV = \int_V \boldsymbol{d}^T \boldsymbol{C} \dot{\boldsymbol{d}} \, dV = \\ \int_\Omega \left[\left(\boldsymbol{u}^T \boldsymbol{C_0} \dot{\boldsymbol{u}} \right) + \left(\boldsymbol{u}^T \boldsymbol{C_1} \dot{\boldsymbol{\theta}} \right) + \left(\boldsymbol{\theta}^T \boldsymbol{C_1}^T \dot{\boldsymbol{u}} \right) + \left(\boldsymbol{\theta}^T \boldsymbol{C_2} \dot{\boldsymbol{\theta}} \right) \right] d\Omega \end{aligned} \tag{26}$$

where $\dot{\boldsymbol{d}}$ is the temporal derivative of the displacement field $\boldsymbol{d}$, namely Eq.(10). The damping matrices $\boldsymbol{C_0}, \boldsymbol{C_1}, \boldsymbol{C_2}$ are defined as

$$\begin{aligned}
\boldsymbol{C_0} &= \int_{\zeta} \boldsymbol{C} \left[1 + k_1 \left(\zeta + \bar{\zeta}\right)\right] \left[1 + k_2 \left(\zeta + \bar{\zeta}\right)\right] d\zeta \\
\boldsymbol{C_1} &= \int_{\zeta} \boldsymbol{C} \mathcal{L} \left(\zeta + \bar{\zeta}\right) \left[1 + k_1 \left(\zeta + \bar{\zeta}\right)\right] \left[1 + k_2 \left(\zeta + \bar{\zeta}\right)\right] d\zeta \\
\boldsymbol{C_2} &= \int_{\zeta} \mathcal{L}^T \boldsymbol{C} \mathcal{L} \left(\zeta + \bar{\zeta}\right)^2 \left[1 + k_1 \left(\zeta + \bar{\zeta}\right)\right] \left[1 + k_2 \left(\zeta + \bar{\zeta}\right)\right] d\zeta
\end{aligned} \tag{27}$$

E. Edge continuity conditions

Let Γ_{pq} be the common edge along the two contiguous shells denoted by $\langle p \rangle$ and $\langle q \rangle$. The joining conditions along this edge require displacement continuity and traction equilibrium. The displacement continuity on Γ_{pq} is implemented requiring that: (i) the modeling plane translations of the two contiguous shells have equal components in the global reference system $\mathcal{R}$, (ii) the rotations around the global axes x_i of the two contiguous shells are equal. These considerations give

$$\boldsymbol{\Lambda}_u^{\langle p \rangle} \boldsymbol{u}^{\langle p \rangle} = \boldsymbol{\Lambda}_u^{\langle q \rangle} \boldsymbol{u}^{\langle q \rangle} \qquad \text{on } \Gamma_{pq} \tag{28a}$$

$$\boldsymbol{\Lambda}_{\vartheta}^{\langle p \rangle} \boldsymbol{\vartheta}^{\langle p \rangle} = \boldsymbol{\Lambda}_{\vartheta}^{\langle q \rangle} \boldsymbol{\vartheta}^{\langle q \rangle} \qquad \text{on } \Gamma_{pq} \tag{28b}$$

where $\boldsymbol{\Lambda}_{\alpha}^{\langle r \rangle}$ are suitable transformation matrices from the local to the global reference systems, which contain the directional cosines between the axes x_i and $\xi_i^{\langle k \rangle}$. It is worth nothing that by introducing the drilling rotation, one assumes that rotations around the local $\zeta^{\langle k \rangle}$-axis of the shell are admitted despite their non-influence on the shell's displacement field. This process allows all of the possible cases of edge rotation continuity to be treated by a single formula that is Eq.(28b). Indeed, in Eq. (28b) three-component rotations vectors are used and each rotation component of the first shell can match a corresponding rotation of the second shell [43]. For the case of an edge shared across multiple shells, Eqs. (28) are written for all possible coupled combinations of shells consisting of a fixed domain and others. Regarding traction equilibrium, these reduce to the equilibrium of the boundary resultant forces and moments expressed in terms of their components along and around the global references axes, respectively. Therefore

$$\sum_i \boldsymbol{\Lambda}_u^{\langle i \rangle} \widetilde{\boldsymbol{N}}^{\langle i \rangle} = \boldsymbol{0} \tag{29a}$$

$$\sum_i \boldsymbol{\Lambda}_{\vartheta}^{\langle i \rangle} \widetilde{\boldsymbol{M}}^{\langle i \rangle} = \boldsymbol{0} \tag{29b}$$

where the summation involves all of the shells joined at the considered edge.

F. Governing equations

Upon substitution of Eq.(18), Eq.(20), Eq.(23), Eq. (26) and Eq. (29) into Eq.(16), integrating by parts with respect to time, invoking the condition of zero variation at the beginning and end of the time interval, the governing equations of the assembled structure are written as

$$
\begin{aligned}
\int_{t_1}^{t_2} \Bigg\{ & \sum_{k=1}^{R_D} \int_{\Omega^{\langle k \rangle}} \Big[\delta \boldsymbol{u}^{\langle k \rangle T} \left(\boldsymbol{I_0}^{\langle k \rangle} \ddot{\boldsymbol{u}}^{\langle k \rangle} + \boldsymbol{I_1}^{\langle k \rangle} \ddot{\boldsymbol{\vartheta}}^{\langle k \rangle} \right) + \\
& \qquad \delta \boldsymbol{\vartheta}^{\langle k \rangle T} \left(\boldsymbol{I_1}^{\langle k \rangle} \ddot{\boldsymbol{u}}^{\langle k \rangle} + \boldsymbol{I_2}^{\langle k \rangle} \ddot{\boldsymbol{\vartheta}}^{\langle k \rangle} \right) \Big] d\Omega + \\
& \sum_{k=1}^{R_D} \int_{\Omega^{\langle k \rangle}} \Big[\delta \boldsymbol{u}^{\langle k \rangle T} \left(\boldsymbol{C_0}^{\langle k \rangle} \dot{\boldsymbol{u}}^{\langle k \rangle} + \boldsymbol{C_1}^{\langle k \rangle} \dot{\boldsymbol{\vartheta}}^{\langle k \rangle} \right) + \\
& \qquad \delta \boldsymbol{\vartheta}^{\langle k \rangle T} \left(\boldsymbol{C_1}^{T\langle k \rangle} \dot{\boldsymbol{u}}^{\langle k \rangle} + \boldsymbol{C_2}^{\langle k \rangle} \dot{\boldsymbol{\vartheta}}^{\langle k \rangle} \right) \Big] d\Omega + \\
& \sum_{k=1}^{R_D} \int_{\Omega^{\langle k \rangle}} \Big[\delta \boldsymbol{u}^{\langle k \rangle T} \mathscr{D}_{p\,u}^{\langle k \rangle T} \left(\boldsymbol{A}^{\langle k \rangle} \mathscr{D}_{p\,u}^{\langle k \rangle} \boldsymbol{u}^{\langle k \rangle} + \boldsymbol{B}^{\langle k \rangle} \mathscr{D}_{p\,\vartheta}^{\langle k \rangle} \boldsymbol{\vartheta}^{\langle k \rangle} \right) + \\
& \qquad \delta \boldsymbol{\vartheta}^{\langle k \rangle T} \mathscr{D}_{p\,\vartheta}^{\langle k \rangle T} \left(\boldsymbol{B}^{\langle k \rangle} \mathscr{D}_{p\,u}^{\langle k \rangle} \boldsymbol{u}^{\langle k \rangle} + \boldsymbol{D}^{\langle k \rangle} \mathscr{D}_{p\,\vartheta}^{\langle k \rangle} \boldsymbol{\vartheta}^{\langle k \rangle} \right) + \\
& \qquad \delta \boldsymbol{u}^{\langle k \rangle T} \mathscr{D}_{n\,u}^{\langle k \rangle T} \left(\boldsymbol{A}_S^{\langle k \rangle} \mathscr{D}_{n\,u}^{\langle k \rangle} \boldsymbol{u}^{\langle k \rangle} + \boldsymbol{A}_S^{\langle k \rangle} \mathscr{D}_{n\,\vartheta}^{\langle k \rangle} \boldsymbol{\vartheta}^{\langle k \rangle} \right) + \\
& \qquad \delta \boldsymbol{\vartheta}^{\langle k \rangle T} \mathscr{D}_{n\,\vartheta}^{\langle k \rangle T} \left(\boldsymbol{A}_S^{\langle k \rangle} \mathscr{D}_{n\,u}^{\langle k \rangle} \boldsymbol{u}^{\langle k \rangle} + \boldsymbol{A}_S^{\langle k \rangle} \mathscr{D}_{n\,\vartheta}^{\langle k \rangle} \boldsymbol{\vartheta}^{\langle k \rangle} \right) \Big] d\Omega - \\
& \sum_{k=1}^{R_D} \int_{\Omega^{\langle k \rangle}} \left(\delta \boldsymbol{u}^{\langle k \rangle T} \boldsymbol{q}^{\langle k \rangle} + \delta \boldsymbol{\vartheta}^{\langle k \rangle T} \boldsymbol{m}^{\langle k \rangle} \right) d\Omega - \\
& \sum_{k=1}^{R_D} \int_{\partial\Omega_l^{\langle k \rangle}} \left(\delta \boldsymbol{u}^{\langle k \rangle T} \bar{\boldsymbol{N}}^{\langle k \rangle} + \delta \boldsymbol{\vartheta}^{\langle k \rangle T} \bar{\boldsymbol{M}}^{\langle k \rangle} \right) d\partial\Omega - \\
& \sum_{k=1}^{R_D} \int_{\partial\Omega_c^{\langle k \rangle}} \Big[\delta \boldsymbol{u}^{\langle k \rangle T} \left(\Xi_u^{\langle k \rangle T} \boldsymbol{\omega}_u^{\langle k \rangle} \Xi_u^{\langle k \rangle} \boldsymbol{u}^{\langle k \rangle} + \Xi_u^{\langle k \rangle T} \boldsymbol{\omega}_u^{\langle k \rangle} \Xi_u^{\langle k \rangle} \bar{\boldsymbol{u}}^{\langle k \rangle} \right) + \\
& \qquad \delta \boldsymbol{\vartheta}^{\langle k \rangle T} \left(\Xi_\vartheta^{\langle k \rangle T} \boldsymbol{\omega}_\vartheta^{\langle k \rangle} \Xi_\vartheta^{\langle k \rangle} \boldsymbol{\vartheta}^{\langle k \rangle} + \Xi_\vartheta^{\langle k \rangle T} \boldsymbol{\omega}_\vartheta^{\langle k \rangle} \Xi_\vartheta^{\langle k \rangle} \bar{\boldsymbol{\vartheta}}^{\langle k \rangle} \right) \Big] d\partial\Omega + \\
& \sum_{p=1}^{R_D-1} \sum_{q=p+1}^{R_D} \int_{\Gamma_{pq}} \frac{1}{2} \left[\Lambda_u^{\langle p \rangle} \boldsymbol{u}^{\langle p \rangle} - \Lambda_u^{\langle q \rangle} \boldsymbol{u}^{\langle q \rangle} \right]^T \boldsymbol{\omega}_u^{\langle p,q \rangle} \left[\Lambda_u^{\langle p \rangle} \boldsymbol{u}^{\langle p \rangle} - \Lambda_u^{\langle q \rangle} \boldsymbol{u}^{\langle q \rangle} \right] d\Gamma + \\
& \sum_{p=1}^{R_D-1} \sum_{q=p+1}^{R_D} \int_{\Gamma_{pq}} \frac{1}{2} \left[\Lambda_\vartheta^{\langle p \rangle} \boldsymbol{\vartheta}^{\langle p \rangle} - \Lambda_\vartheta^{\langle q \rangle} \boldsymbol{\vartheta}^{\langle q \rangle} \right]^T \boldsymbol{\omega}_\vartheta^{\langle p,q \rangle} \left[\Lambda_\vartheta^{\langle p \rangle} \boldsymbol{\vartheta}^{\langle p \rangle} - \Lambda_\vartheta^{\langle q \rangle} \boldsymbol{\vartheta}^{\langle q \rangle} \right] d\Gamma \Bigg\} dt = 0
\end{aligned}
\tag{30}
$$

where R_D is the number of shell-like domains used in the domain decomposition of the structure and $\boldsymbol{\omega}_u^{\langle k \rangle}$, $\boldsymbol{\omega}_\vartheta^{\langle k \rangle}$, $\boldsymbol{\omega}_u^{\langle p,q \rangle}$ and $\boldsymbol{\omega}_\vartheta^{\langle p,q \rangle}$ are diagonal matrices containing the penalty coefficients. Note that the joining constraints are algorithmically expressed considering all of the possible coupled combinations of shells in the structure through the double summation introduced in Eq.(30); if the shells $\langle p \rangle$ and $\langle q \rangle$ do not share a joining edge then Γ_{pq} has zero measure and thus the corresponding constraint actually become meaningless. Similar considerations hold for the essential boundary condition constraints, which are introduced for all of the shells and give no contribution if $\partial\Omega_c^{\langle k \rangle}$ has zero measure.

III. Ritz approximation

A. Generalized displacements and strain-displacements relations

The generalized displacements of the shell in the local $\widetilde{\mathcal{R}}(\xi_1, \xi_2, \zeta)$ reference system are approximated by a series of trial functions as

$$\tau = \sum_{i=1}^{M_\tau} \sum_{j=1}^{N_\tau} p_i(\xi_1)\, p_j(\xi_2)\, C_{\tau_{ij}}(t) = \boldsymbol{\Psi}_\tau(\xi_1, \xi_2) \boldsymbol{C}_\tau(t) \tag{31}$$

In Eq. (31) the $1 \times N_\tau M_\tau$ row vectors $\boldsymbol{\Psi}_\tau$, with $\tau \in \{u_1, u_2, u_3, \vartheta_1, \vartheta_2, \vartheta_3\}$, have components $\psi_{\tau_{(i-1)M_\tau + j}} = p_i(\xi_1) p_j(\xi_2)$ whereas the $N_\tau M_\tau \times 1$ column vectors $\boldsymbol{C}_\tau(t)$ contains unknown coefficients that are functions of time.

According to Section II.B, the generalized displacements are conveniently written as

$$\boldsymbol{u} = \begin{bmatrix} \boldsymbol{\Psi}_{u_1} & \mathbf{0} & \mathbf{0} \\ \mathbf{0} & \boldsymbol{\Psi}_{u_2} & \mathbf{0} \\ \mathbf{0} & \mathbf{0} & \boldsymbol{\Psi}_{u_3} \end{bmatrix} \begin{Bmatrix} \boldsymbol{C}_{u_1} \\ \boldsymbol{C}_{u_2} \\ \boldsymbol{C}_{u_3} \end{Bmatrix} = \begin{bmatrix} \boldsymbol{\phi}_{\boldsymbol{u_1}} \\ \boldsymbol{\phi}_{\boldsymbol{u_2}} \\ \boldsymbol{\phi}_{\boldsymbol{u_3}} \end{bmatrix} \boldsymbol{U} = \boldsymbol{\Phi}_{\boldsymbol{u}} \boldsymbol{U} \tag{32a}$$

$$\boldsymbol{\vartheta} = \begin{bmatrix} \boldsymbol{\Psi}_{\vartheta_1} & \mathbf{0} & \mathbf{0} \\ \mathbf{0} & \boldsymbol{\Psi}_{\vartheta_2} & \mathbf{0} \\ \mathbf{0} & \mathbf{0} & \boldsymbol{\Psi}_{\vartheta_3} \end{bmatrix} \begin{Bmatrix} \boldsymbol{C}_{\vartheta_1} \\ \boldsymbol{C}_{\vartheta_2} \\ \boldsymbol{C}_{\vartheta_3} \end{Bmatrix} = \begin{bmatrix} \boldsymbol{\phi}_{\boldsymbol{\vartheta_1}} \\ \boldsymbol{\phi}_{\boldsymbol{\vartheta_2}} \\ \boldsymbol{\phi}_{\boldsymbol{\vartheta_3}} \end{bmatrix} \boldsymbol{\Theta} = \boldsymbol{\Phi}_{\boldsymbol{\vartheta}} \boldsymbol{\Theta} \tag{32b}$$

From Eqs (14) one deduces

$$\boldsymbol{\varepsilon} = \mathscr{D}_{p_u} \boldsymbol{u} = \left[\mathscr{D}_{p_u} \boldsymbol{\Phi}_{\boldsymbol{u}} \right] \boldsymbol{U} = \mathcal{B}_{p_U} \boldsymbol{U} \tag{33a}$$

$$\boldsymbol{\kappa} = \mathscr{D}_{p_\vartheta} \boldsymbol{\vartheta} = \left[\mathscr{D}_{p_\vartheta} \boldsymbol{\Phi}_{\boldsymbol{\vartheta}} \right] \boldsymbol{\Theta} = \mathcal{B}_{p_\Theta} \boldsymbol{\Theta} \tag{33b}$$

$$\boldsymbol{\gamma} = \mathscr{D}_{nu} \boldsymbol{u} + \mathcal{L} \boldsymbol{\vartheta} = \left[\mathscr{D}_{nu} \boldsymbol{\Phi}_{\boldsymbol{u}} \right] \boldsymbol{U} + \left[\mathcal{L} \boldsymbol{\Phi}_{\boldsymbol{\vartheta}} \right] \boldsymbol{\Theta} = \mathcal{B}_{n_U} \boldsymbol{U} + \mathcal{B}_{n_\Theta} \boldsymbol{\Theta} \tag{33c}$$

with the corresponding virtual variations

$$\delta\boldsymbol{\varepsilon} = \mathcal{B}_{p_U} \delta \boldsymbol{U} \tag{34a}$$

$$\delta\boldsymbol{\kappa} = = \mathcal{B}_{p_\Theta} \delta \boldsymbol{\Theta} \tag{34b}$$

$$\delta\boldsymbol{\gamma} = \mathcal{B}_{n_U} \delta \boldsymbol{U} + \mathcal{B}_{n_\Theta} \delta \boldsymbol{\Theta} \tag{34c}$$

B. Linear transient system of equation

Upon substitution of Eqs.(32) and (33) into Eqs.(30) and considering the arbitrariness of the virtual displacements $\delta \boldsymbol{U}^{\langle k \rangle}$ and $\delta \boldsymbol{\Theta}^{\langle k \rangle}$, the system of equations of the assembled structure needed for solution can be obtained and expressed in its classical form as

$$\boldsymbol{K}_M \ddot{\boldsymbol{X}} + \boldsymbol{K}_C \dot{\boldsymbol{X}} + \boldsymbol{K} \boldsymbol{X} = \boldsymbol{F}_D + \boldsymbol{F}_L \tag{35}$$

where, $\boldsymbol{K}_M$ and $\boldsymbol{K}_C$ are block diagonal symmetric matrices, $\boldsymbol{K}$ is a block symmetric matrix and $\boldsymbol{X}$, $\dot{\boldsymbol{X}}$ and $\ddot{\boldsymbol{X}}$ are block column vectors that collect all unknown Ritz coefficients and their first and second time derivatives. Likewise, $\boldsymbol{F}_D$ and $\boldsymbol{F}_L$ are block column vectors. The total number of blocks of equations is equal to the total number of shell domains of the assembled structure, R_D. Therefore, for the k-th domain, the k-th block of equations can be written as

$$\begin{aligned}\boldsymbol{K}_M^{\langle k\rangle}\ddot{\boldsymbol{X}}^{\langle k\rangle}+\boldsymbol{K}_C^{\langle k\rangle}\dot{\boldsymbol{X}}^{\langle k\rangle}+\left[\boldsymbol{K}_0^{\langle k\rangle}+\boldsymbol{R}^{\langle k\rangle}+\sum_{\substack{r=1\\ r\neq k}}^{R_D}\boldsymbol{P}_{kr}^{\langle k,k\rangle}\right]\boldsymbol{X}^{\langle k\rangle}-\\ \sum_{\substack{r=1\\ r\neq k}}^{R_D}\left[\boldsymbol{P}_{kr}^{\langle k,r\rangle}\boldsymbol{X}^{\langle r\rangle}\right]=\boldsymbol{F}_D^{\langle k\rangle}+\boldsymbol{F}_L^{\langle k\rangle}\end{aligned}\qquad \text{for}\quad k=1,\cdots,R_D \tag{36}$$

where

$$\boldsymbol{K}_M^{\langle k\rangle}=\begin{bmatrix}\int_{\Omega^{\langle k\rangle}}(\boldsymbol{\Phi_u}^{\langle k\rangle T}\boldsymbol{I_0}^{\langle k\rangle}\boldsymbol{\Phi_u}^{\langle k\rangle})\,d\Omega & \int_{\Omega^{\langle k\rangle}}(\boldsymbol{\Phi_u}^{\langle k\rangle T}\boldsymbol{I_1}\boldsymbol{\Phi_\vartheta}^{\langle k\rangle})\,d\Omega\\ \int_{\Omega^{\langle k\rangle}}(\boldsymbol{\Phi_\vartheta}^{\langle k\rangle T}\boldsymbol{I_1}^{\langle k\rangle}\boldsymbol{\Phi_u}^{\langle k\rangle})\,d\Omega & \int_{\Omega^{\langle k\rangle}}(\boldsymbol{\Phi_\vartheta}^{\langle k\rangle T}\boldsymbol{I_2}^{\langle k\rangle}\boldsymbol{\Phi_\vartheta}^{\langle k\rangle})\,d\Omega\end{bmatrix} \tag{37a}$$

$$\boldsymbol{K}_C^{\langle k\rangle}=\begin{bmatrix}\int_{\Omega^{\langle k\rangle}}(\boldsymbol{\Phi_u}^{\langle k\rangle T}\boldsymbol{C_0}^{\langle k\rangle}\boldsymbol{\Phi_u}^{\langle k\rangle})\,d\Omega & \int_{\Omega^{\langle k\rangle}}(\boldsymbol{\Phi_u}^{\langle k\rangle T}\boldsymbol{C_1}\boldsymbol{\Phi_\vartheta}^{\langle k\rangle})\,d\Omega\\ \int_{\Omega^{\langle k\rangle}}(\boldsymbol{\Phi_\vartheta}^{\langle k\rangle T}\boldsymbol{C_1}^{T\langle k\rangle}\boldsymbol{\Phi_u}^{\langle k\rangle})\,d\Omega & \int_{\Omega^{\langle k\rangle}}(\boldsymbol{\Phi_\vartheta}^{\langle k\rangle T}\boldsymbol{C_2}^{\langle k\rangle}\boldsymbol{\Phi_\vartheta}^{\langle k\rangle})\,d\Omega\end{bmatrix} \tag{37b}$$

$$\boldsymbol{K}_0^{\langle k\rangle}=\begin{bmatrix}\int_{\Omega^{\langle k\rangle}}\left(\mathcal{B}_{pU}^{\langle k\rangle T}\boldsymbol{A}^{\langle k\rangle}\mathcal{B}_{pU}^{\langle k\rangle}+\mathcal{B}_{nU}^{\langle k\rangle T}\boldsymbol{A}_S^{\langle k\rangle}\mathcal{B}_{nU}^{\langle k\rangle}\right)d\Omega & \int_{\Omega^{\langle k\rangle}}\left(\mathcal{B}_{pU}^{\langle k\rangle T}\boldsymbol{B}^{\langle k\rangle}\mathcal{B}_{p\Theta}^{\langle k\rangle}+\mathcal{B}_{nU}^{\langle k\rangle T}\boldsymbol{A}_S^{\langle k\rangle}\mathcal{B}_{n\Theta}^{\langle k\rangle}\right)d\Omega\\ \int_{\Omega^{\langle k\rangle}}\left(\mathcal{B}_{p\Theta}^{\langle k\rangle T}\boldsymbol{B}^{\langle k\rangle T}\mathcal{B}_{pU}^{\langle k\rangle}+\mathcal{B}_{n\Theta}^{\langle k\rangle T}\boldsymbol{A}_S^{\langle k\rangle}\mathcal{B}_{nU}^{\langle k\rangle}\right)d\Omega & \int_{\Omega^{\langle k\rangle}}\left(\mathcal{B}_{p\Theta}^{\langle k\rangle T}\boldsymbol{D}^{\langle k\rangle}\mathcal{B}_{p\Theta}^{\langle k\rangle}+\mathcal{B}_{n\Theta}^{\langle k\rangle T}\boldsymbol{A}_S^{\langle k\rangle}\mathcal{B}_{n\Theta}^{\langle k\rangle}\right)d\Omega\end{bmatrix} \tag{37c}$$

$$\boldsymbol{R}^{\langle k\rangle}=\begin{bmatrix}\int_{\partial\Omega_c^{\langle k\rangle}}\left(\boldsymbol{\Phi}_u^{\langle k\rangle T}\boldsymbol{\Xi}_u^{\langle k\rangle T}\boldsymbol{\omega}_u^{\langle k\rangle}\boldsymbol{\Xi}_u^{\langle k\rangle}\boldsymbol{\Phi}_u\right)d\partial\Omega & \boldsymbol{0}\\ \boldsymbol{0} & \int_{\partial\Omega_c^{\langle k\rangle}}\left(\boldsymbol{\Phi}_\vartheta^{\langle k\rangle T}\boldsymbol{\Xi}_\vartheta^{\langle k\rangle T}\boldsymbol{\omega}_\vartheta^{\langle k\rangle}\boldsymbol{\Xi}_\vartheta^{\langle k\rangle}\boldsymbol{\Phi}_\vartheta^{\langle k\rangle}\right)d\partial\Omega\end{bmatrix} \tag{37d}$$

$$\boldsymbol{P}_{pq}^{\langle r,s\rangle}=\begin{bmatrix}\int_{\Gamma_{pq}}\left(\boldsymbol{\Phi}_u^{\langle r\rangle T}\boldsymbol{\Lambda}_u^{\langle r\rangle T}\boldsymbol{\omega}_u^{\langle pq\rangle}\boldsymbol{\Lambda}_u^{\langle s\rangle}\boldsymbol{\Phi}_u^{\langle s\rangle}\right)d\Gamma & \boldsymbol{0}\\ \boldsymbol{0} & \int_{\Gamma_{pq}}\left(\boldsymbol{\Phi}_\vartheta^{\langle r\rangle T}\boldsymbol{\Lambda}_\vartheta^{\langle r\rangle T}\boldsymbol{\omega}_\vartheta^{\langle pq\rangle}\boldsymbol{\Lambda}_\vartheta^{\langle s\rangle}\boldsymbol{\Phi}_\vartheta^{\langle s\rangle}\right)d\Gamma\end{bmatrix} \tag{37e}$$

$$\boldsymbol{F}_D^{\langle k\rangle}=\begin{Bmatrix}\int_{\Omega^{\langle k\rangle}}\left(\boldsymbol{\Phi}_u^{\langle k\rangle T}\boldsymbol{q}^{\langle k\rangle}\right)d\Omega\\ \int_{\Omega^{\langle k\rangle}}\left(\boldsymbol{\Phi}_\vartheta^{\langle k\rangle T}\boldsymbol{m}^{\langle k\rangle}\right)d\Omega\end{Bmatrix} \tag{37f}$$

$$\boldsymbol{F}_L^{\langle k\rangle}=\begin{Bmatrix}\int_{\partial\Omega_c^{\langle k\rangle}}\boldsymbol{\Phi}_u^{\langle k\rangle T}\boldsymbol{\Xi}_u^{\langle k\rangle}\bar{\boldsymbol{u}}^{\langle k\rangle}+\int_{\partial\Omega_l^{\langle k\rangle}}\boldsymbol{\Phi}_u^{\langle k\rangle T}\bar{\boldsymbol{N}}^{\langle k\rangle}\\ \int_{\partial\Omega_c^{\langle k\rangle}}\boldsymbol{\Phi}_\vartheta^{\langle k\rangle T}\boldsymbol{\Xi}_\vartheta^{\langle k\rangle}\bar{\boldsymbol{\vartheta}}^{\langle k\rangle}+\int_{\partial\Omega_l^{\langle k\rangle}}\boldsymbol{\Phi}_\vartheta^{\langle k\rangle T}\bar{\boldsymbol{M}}^{\langle k\rangle}\end{Bmatrix} \tag{37g}$$

Thus Eq.(35) can be solved with the Newmark numerical time integration method. Note that by using the penalty method [44] to enforce natural boundary conditions the dimension of the stiffness operator remains unchanged. In fact, only the sparsity of the resulting stiffness matrix $\boldsymbol{K}$ reduces due to the presence of off-diagonal terms. Furthermore, properties including symmetry and positive-definiteness remain.

C. Linear free vibration system of equation

The undamped free vibration eigenvalue problem is straightforwardly retrieved from Eq.(35), namely

$$\left[\boldsymbol{K} - \omega^2 \boldsymbol{K}_M\right]\boldsymbol{X} = 0 \tag{38}$$

where the eigenvalue ω^2 is the circular frequency and the eigenvectors $\boldsymbol{X}$ are the Ritz coefficients associated with the vibration mode. As for Eq.(35), for the k-th domain, the k-th block of equations can be written as

$$\begin{aligned} &\left[\boldsymbol{K}_0^{\langle k\rangle} + \boldsymbol{R}^{\langle k\rangle} + \sum_{\substack{r=1\\ r\neq k}}^{R_D} \boldsymbol{P}_{kr}^{\langle k,k\rangle} - \omega^2 \boldsymbol{K}_M^{\langle k\rangle}\right]\boldsymbol{X}^{\langle k\rangle} - \\ &\qquad \sum_{\substack{r=1\\ r\neq k}}^{R_D} \left[\boldsymbol{P}_{kr}^{\langle k,r\rangle}\boldsymbol{X}^{\langle r\rangle}\right] = 0 \end{aligned} \qquad \text{for} \quad k = 1, \cdots, R_D \tag{39}$$

IV. Implementation and modeling strategies

The proposed Ritz approach has been implemented in an analysis tool with the following features. The trial functions $\psi_i(\xi_1, \xi_2)$ are constructed by using orthogonal polynomials whose efficiency and performances for this kind of formulation are well established [45]. In particular, one sets

$$\psi_{(nM+m)} = \varphi_n(\xi_1)\,\chi_m(\xi_2) \qquad n = 0, ..., N; \quad m = 0, ..., M \tag{40}$$

where M and N are the order of the approximated variable expansion and $\varphi_n(\xi_1)$ and $\chi_m(\xi_2)$ are one-dimensional orthogonal polynomials. For the present paper, φ_n and χ_m are chosen as Legendre orthogonal polynomials

$$\varphi_n(\lambda) = \chi_n(\lambda) = \frac{1}{2^n n!}\frac{d^n}{d\lambda^n}\left[\left(\lambda^2 - 1\right)^n\right] \tag{41}$$

Jacobi and Chebyshev orthogonal polynomials [46] have also been tested without appreciable variations in results. The trial functions provided by Eq.(40) generally do not satisfy the kinematic boundary conditions, which are explicitly imposed as a constraint in the variational statement (see Eq.(30)). Different approximation schemes based on trial functions that satisfy the kinematic boundary conditions could also be employed. Nevertheless, the trial functions given by Eqs.(40) and (41) allow simple implementation and efficient evaluation of the line integrals involved in the system matrices. The penalty coefficients are chosen considering them as artificial springs distributed along the shell joints, whose stiffnesses per unit length are set as 10^S-times the mean of a representative stiffness coefficient, evaluated for the involved contiguous shells. Actually, for the translational springs the representative stiffness coefficient is chosen as the maximum Young's modulus of the laminate, whereas for the rotational springs it is chosen to be the maximum value of

the laminate Young's modulus times the square of the shell thickness. As with literature findings [47, 48], sensitivity analyses showed that the results do not appreciably vary for S between 3 and 7; therefore in the implementation of the numerical tool a value $S = 5$ has been used. Offsets $\bar{\zeta}^{\langle k \rangle}$ can be used to define the relative position along the thickness of contiguous shells. They also select the modeling plane that defines the physical meaning of the generalized displacements and on which loads, kinematic constraints and edge continuity are applied (see Fig.3). The domain

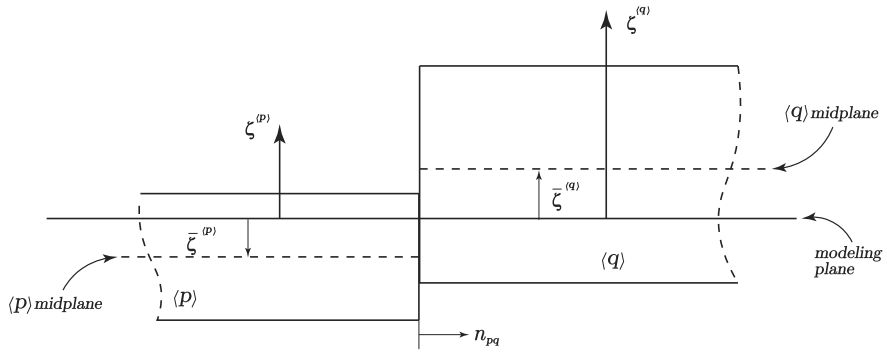

Figure 3 Edges of contiguous shells and offsets

integrals as well as the boundary integrals are numerically computed by Legendre-Gauss quadrature formulae whose order is suitably set according to the order of the employed polynomials for satisfactory accuracy [49]. Their evaluation requires the description of the shell's constitutive law that for VS laminates depends on the reference surface coordinates through the variation of the fiber orientation θ that is assumed to be

$$\theta^{\langle k \rangle}(x_1^{\langle k \rangle},\ x_2^{\langle k \rangle}) = \theta^{\langle k \rangle}(\xi_1^{\langle k \rangle},\ \xi_2^{\langle k \rangle}) = \theta_0{}^{\langle k \rangle} + \sum_{i=0}^{M} \psi_i^{\langle k \rangle} C_{\theta_i}^{\langle k \rangle} \tag{42}$$

where $\theta_0^{\langle k \rangle}$ is a constant fiber angle. The unknown coefficients C_{θ_i} are determined by collocation of Eq. (42) at a set of $(M + 1)$ reference points in the shell domain where the fiber angles are given as input data. In the current implementation of the computer code, linear variation ($M = 1$) of fiber orientation angles is considered although more general distribution can be straightforwardly considered. In particular, fiber angle variations as introduced in Ref. [2] are considered. Considering the possible complexity of fiber orientations in thin-walled structures, to simplify the data preparation, the fiber angle variation of each shell of the structure is referred to the vector $\hat{\boldsymbol{n}}_0^{\langle k \rangle}$, which is tangent to the modelling plane in the point P_0 and together with the surface normal in P_0 defines the zero fiber orientation plane Γ_0. Hence, referring to Fig.4, let us consider a reference curvilinear axis r as the intersection between the reference surface of the shell and the plane Γ which is obtained by rotating Γ_0 along the normal in P_0 by an angle θ_0. Consider a point A to be the origin of the axis r and θ'_A be the angle between the fiber and the direction r at the point A. Moving along the r-axis, at a characteristic distance d from the point A, the fiber angle becomes θ'_B at the point B. The fiber angle along

the r-axis is assumed to vary as

$$\theta(r) = \theta_0 + (\theta'_B - \theta'_A)\frac{\tilde{r}}{d} + \theta'_A \tag{43}$$

where $\tilde{r}$ can be specified as $\tilde{r} = r$ or $\tilde{r} = |r|$. It is worth noting that these definitions allow both symmetric and nonsymmetric variations of the fibres angle to be described with respect to the chosen starting point. Eq. (43) defines the fiber angles on the r-axis; it is assumed that the fiber orientation at other points in the domain is obtained by shifting this basic path in a direction perpendicular to the r-axis. Thus the fiber orientation becomes a function of both local in-plane coordinates, namely $\theta = \theta(\xi_1, \xi_2)$. According to this kind of fiber pattern, a VS ply is described by the notation $\theta_0 + \langle \theta'_A | \theta'_B \rangle$ if $\tilde{r} = |r|$ or $\theta_0 + \langle\langle \theta'_A | \theta'_B \rangle\rangle$ if $\tilde{r} = r$. The laminate layup is then described by the conventional representation assuming that a ± sign in front of either θ_0 or $\langle \theta'_A | \theta'_B \rangle$ or $\langle\langle \theta'_A | \theta'_B \rangle\rangle$ means that there are two adjacent layers with equal and opposite variation of the fiber angle. This notation actually extends that introduced in Ref. [2]. In

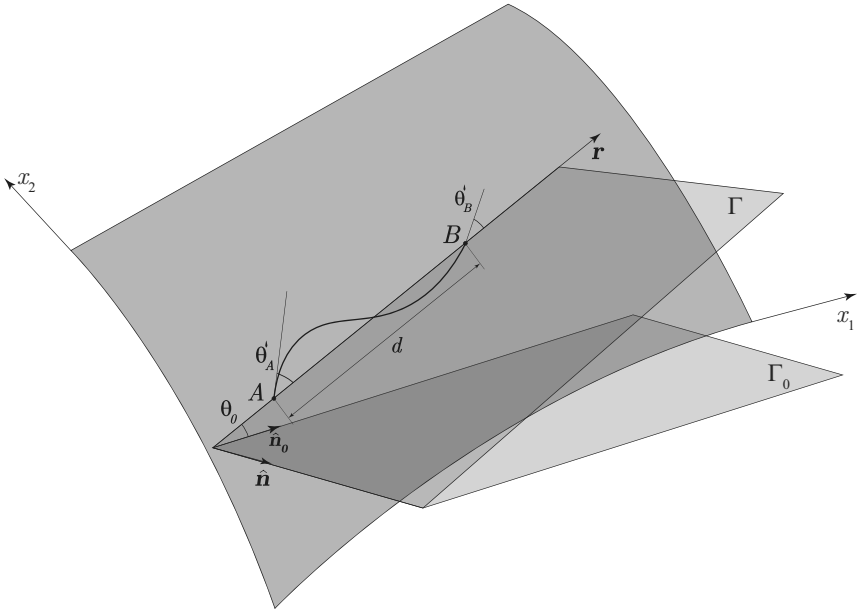

Figure 4 Shell with fiber orientation angle definitions

the implementation of the linear transient solution procedures, the following assumptions are considered: (i) the model used for structural damping is viscous and frequency dependant; (ii) the approach is formulated for the linear response of the structure. Hence, in the framework of the Rayleigh damping model, the damping matrix of the system, namely $\boldsymbol{K}_C$ in Eq.(35), is numerically evaluated as a linear combination of the mass and stiffness matrices as

$$\boldsymbol{K}_C = \alpha \boldsymbol{K}_M + \beta \boldsymbol{K} \tag{44}$$

The coefficients α and β are determined from user-specified damping ratios ζ_i and ζ_j for the i-th and j-th modes respectively by solving the system

$$\frac{1}{2}\begin{bmatrix} \frac{1}{\omega_i} & \omega_i \\ \frac{1}{\omega_j} & \omega_j \end{bmatrix} \begin{Bmatrix} \alpha \\ \beta \end{Bmatrix} = \begin{Bmatrix} \zeta_i \\ \zeta_j \end{Bmatrix} \tag{45}$$

which then allow for the evaluation of damping ratios for all natural modes of vibration of the structure. Finally, the linear transient governing equations are solved by commonly used Newmark time integration schemes.

V. Validation and results

In this section, free vibration and linear transient analyses of VS shell structures are carried out and results are compared with literature and FE solutions. To show the capabilities of the present method, original results of free vibration and transient analyses of VS stiffened shell structures are presented for two case studies: a VS stiffened doubly-curved shell and a VS stiffened variable curvature shell. Those geometries are chosen as representative of typical aerospace structures such as generally curved stiffened aircraft panels and nacelles. Due to absence of literature results for VS stiffened shells, the results are compared with FE. Note that the chosen layups and structural configurations do not represent optimized designs for the chosen load-cases, rather serve to demonstrate the robustness and wide applicability of the modelling approach. All the reported FE and Ritz results follow a convergence study that is not fully reported in the following for the sake of conciseness.

A. Free Vibrations

In order to benchmark the proposed method, a convergence analysis is carried out first considering simple cylindrical shell geometries. The general cylindrical shell geometry is depicted in Fig.5. Two test cases $TC1$ and $TC2$ with

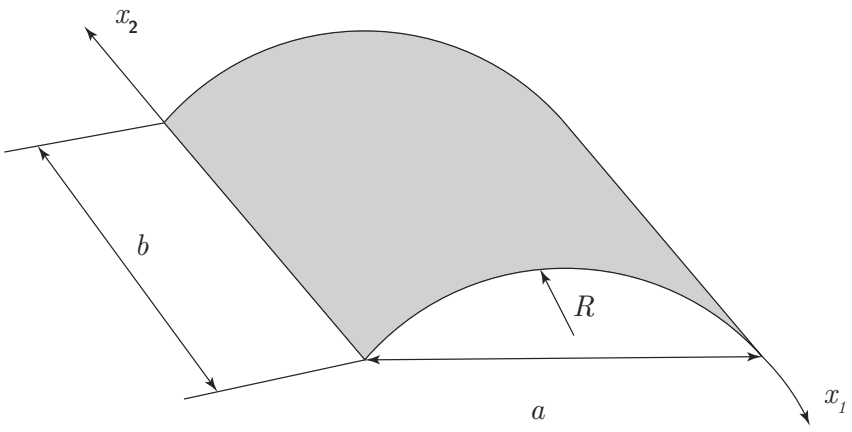

Figure 5 Cylindrical shell geometry

different radius/thickness ratios are studied. For both $TC1$ and $TC2$, the material properties $CFRP_1$ shown in Table 1 are considered and a fully clamped boundary condition holds along all of the edges. Details about the geometry and layups are shown in Table 2 and Table 4 for $TC1$ and $TC2$ respectively. Referring to Fig. 5, all fiber angle variations are considered with respect to a direction vector $\hat{\boldsymbol{n}}_{\mathbf{0}}$ tangent to the curved edge of the cylinder in $x_1 = 0$ and the characteristic distance d starts from the edge midpoint and equals half of the curved edge's length. Values of the first ten natural frequencies of the shell $TC1$ are reported in Table 3 for increasing number of polynomials $R_P = \{8, 10, 12\}$, while values of the lowest ten natural frequencies of the shell $TC2$ are reported in Table 5 for increasing number of domains $R_D = \{1, 2, 4\}$ and $R_P = 8$. The multi-domain analyses are carried out considering equally sized domains. Note, this convergence study varying R_D and R_P is carried out just to verify the ability and the accuracy of the penalty method herein employed to apply continuity conditions between Ritz domains. In fact, according to the essential idea behind the Ritz method, the present approach relies just on the number of trial functions used in the approximation of the displacement field in order to improve the accuracy of the solution. The analysis of the results shows that the maximum relative difference with respect to literature results is 0.5% for $TC1$ and less than 1.0% for $TC2$ for most of the first ten natural frequencies. It is emphasized that for $TC2$ a difference of 2.2% is observed between the present results and [50] where a thin shell formulation is considered. Comparing the two sets of results from Table 3 and Table 5, it is evident that the result of increasing R_P or R_D is similar in terms of the convergence trend. However, increasing R_P is more efficient rather than increasing the number of domains R_D. In fact, the solution converges uniformly by increasing R_P and $R_P = 12$ with $R_D = 1$ also being adequate to obtain good accuracy in the higher frequency range. This discussion highlights that the best modeling strategy for the proposed approach is to model the structure with the minimum number of domains and use higher R_P to achieve converged results.

Table 1 Mechanical properties of material $CFRP_1$

E_1	E_2	G_{12}	ν_{12}	ρ
$126.3\,[GPa]$	$8.765\,[GPa]$	$4.92\,[GPa]$	0.3	$1600.0\,[^{kg}/_{m^3}]$

Table 2 Geometry, layup and boundary conditions of a VS shallow cylindrical shell

Geometry:	$a = 1.0\,[m] \quad b = 2.0\,[m] \quad R = 4.0\,[m] \quad h = 0.01\,[m]$
Layup:	$\left[\langle 22.5\vert 45\rangle / \langle -22.5\vert -45\rangle\right]_s$
BC:	$u_1 = u_2 = u_3 = \vartheta_1 = \vartheta_2 = 0$ at $x_1 = \pm^a/_2$
	$u_1 = u_2 = u_3 = \vartheta_1 = \vartheta_2 = 0$ at $x_2 = \pm^b/_2$

In order to show the capability of the present method for complex VS structures, two geometries, representative of typical aerospace structures, are studied, namely a variable curvature VS stiffened shell, $TC3$, shown in Fig.6 and a spherical stiffened shell, $TC4$, shown in 8. Referring to the stiffened variable curvature shell $TC3$, details of geometry

Table 3 Natural frequencies (Hz) of a VS shallow cylindrical shell for increasing number of domains R_D and fixed $R_P = 8$.

Mode	$R_D = 1$	$R_D = 2$	$R_D = 4$	Ref. [24]	Ref. [50]
1	1142.4	1141.8	1140.4	1145.856	1154
2	1250.7	1249.8	1249.0	1252.760	1258
3	1345.5	1344.3	1344.4	1346.969	1350
4	1360.7	1360.3	1361.0	1362.994	1366
5	1481.7	1477.7	1477.4	1480.398	1485
6	1497.2	1487.7	1487.6	1490.168	1493
7	1683.7	1645.1	1643.9	1648.284	1652
8	1734.6	1646.4	1646.2	1649.568	1654
9	1906.8	1833.7	1832.8	1838.291	-
10	2150.0	1834.7	1833.0	1838.769	-

Table 4 Geometry, layup and boundary conditions of a VS cylindrical shell

Geometry:	$a = b = 1.0\,[m] \quad R = 2.5\,[m] \quad h = 0.01\,[m]$
Layup:	$\left[\langle 90\vert 45\rangle / \langle -90\vert -45\rangle\right]_s$
BC:	$u_1 = u_2 = u_3 = \vartheta_1 = \vartheta_2 = 0$ at $x_1 = \pm {}^{a}/_{2}$
	$u_1 = u_2 = u_3 = \vartheta_1 = \vartheta_2 = 0$ at $x_2 = \pm {}^{b}/_{2}$

Table 5 Natural frequencies (Hz) of a VS cylindrical shell for increasing number of polynomials R_P.

Mode	$R_P = 8$	$R_P = 10$	$R_P = 12$	Ref. [24]	Ref. [50]
1	1032.1	1016.1	1014.0	1018.500	1024
2	1066.9	1062.5	1061.7	1063.787	1068
3	1511.5	1467.0	1460.9	1471.628	1482
4	1821.2	1813.7	1808.6	1807.712	1827
5	1894.5	1877.5	1873.0	1876.093	1899
6	2203.6	2063.5	1998.5	2007.346	2040
7	2795.8	2317.0	2255.6	2255.490	2300
8	2992.2	2745.4	2648.9	2651.875	2709
9	3129.5	3082.4	2922.4	2893.899	-
10	3272.9	3093.9	3061.1	3060.272	-

are shown in Table 8 and in Fig.6. The layup angle is considered to vary along the x_1 direction (see Fig. 6) only for the panels with a reference distance d starting from the edge midpoint and equal to half the panel width. A straight fiber layup having a reference direction along the x_2 axis is considered for the stiffeners. A ply thickness of $p_{th} = 0.25\,[mm]$ is assumed for all layups and details of the lamination scheme for each domain of the entire structure are reported in Table 8. The material properties $CFRP_1$ are shown in Table 1. The shell structure is clamped on all of the outer edges and the analysis is conducted considering the entire structure to be subdivided in to nine shell domains ($R_D = 9$), namely one domain for each panel, one domain for each stiffener web and two domains for each stiffener flange. For all domains $R_P = 10$ is considered as it provides converged results for the range of frequencies studied with a total number of degrees of freedom that is $DOF_R = 9 \times (10 \times 10 \times 6) = 5400$. In order to verify the accuracy of the solution, Abaqus FE results are taken as reference since no published data was found for stiffened VS shells. In order to model VS shells, the finite element model is generated using a subroutine that assigns an independent constant fiber angle for each mesh element. In particular, a mesh of 25600 $S4R$ elements is used for the analysis, resulting in a total number of degrees of freedom of $DOF_F = 155574$, providing converged results. Table 7 shows the first eight free vibration frequencies. The maximum relative difference with finite element solutions is smaller than 1.5%. Note that the proposed method requested a number of DOF_R that is less than 4% of the degrees of freedom required by FE analysis with a substantial reduction of computational time and without any noticeable loss of accuracy. The good agreement between FE and Ritz results is also shown in Fig. 7 where the first eight mode shapes are presented.

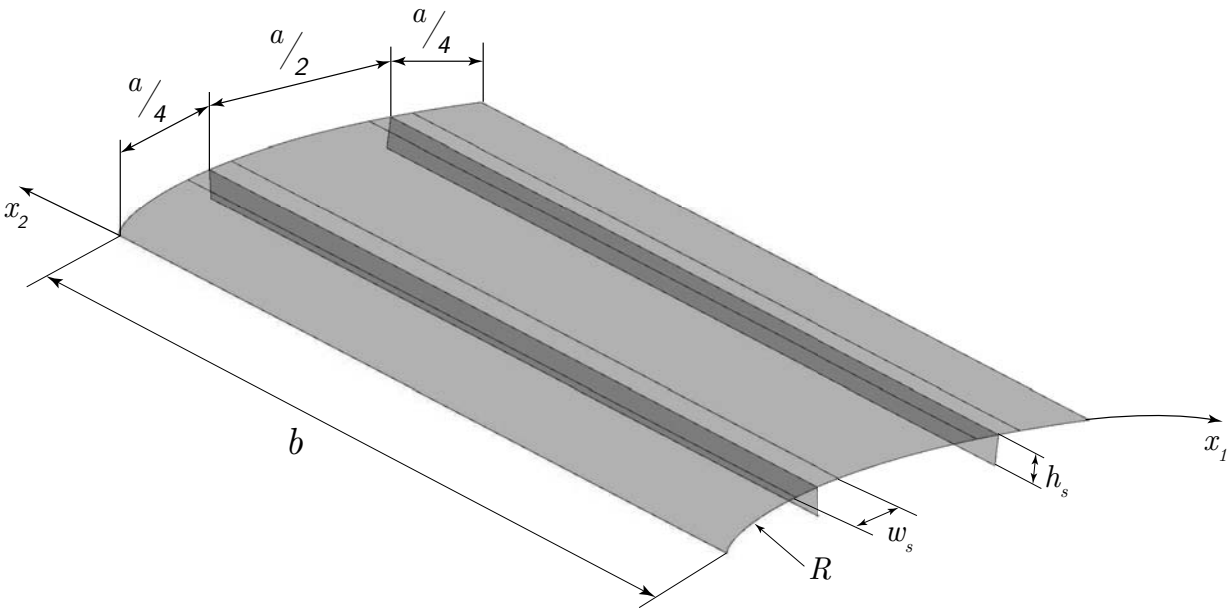

Figure 6 Geometry of a stiffened variable curvature shell

Referring to the stiffened spherical shell $TC4$ shown in Fig.8, the angle of the curvilinear fibers is considered to vary only along the x_1 direction with a characteristic distance d starting from the edge midpoint and equal to half of the panel

Table 6 Geometry, layup and boundary conditions of a VS stiffened variable curvature shell.

Geometry:	$a = 0.1\,[m] \quad b = 0.2\,[m] \quad p_{th} = 0.25\,[mm]$
	$R(x_1) = 0.00929\,{x_1}^2 + 5.989\,x_1 + 275.408\,[mm]$
	$w_s = 0.012\,[m] \quad h_s = 0.007\,[m]$
Layup:	left shell $\left[\langle\langle 45\vert 90\rangle\rangle/\langle\langle -45\vert -90\rangle\rangle/0_2\right]_s$
	central shell $\left[\langle 45\vert 90\rangle/\langle -45\vert -90\rangle/0_2\right]_s$
	right shell $\left[\langle\langle 90\vert 45\rangle\rangle/\langle\langle -90\vert -45\rangle\rangle/0_2\right]_s$
	stiffener flange $\left[\pm 90/0_4/\mp 90/\pm 45/90/0_2/90/\mp 45\right]$
	stiffener web $\left[\pm 45/90/0\right]_s$
BC:	$u_1 = u_2 = u_3 = \vartheta_1 = \vartheta_2 = 0$ at $x_1 = \pm {}^{a}/_{2}$
	$u_1 = u_2 = u_3 = \vartheta_1 = \vartheta_2 = 0$ at $x_2 = \pm {}^{b}/_{2}$

Table 7 Natural frequencies [rad/s] of a VS stiffened variable curvature shell.

Mode	$R_P = 10$	FE	diff%
1	12660.4	12553.1	0.85
2	18606.9	18543.5	0.34
3	20573.9	20251.9	1.58
4	25225.7	24969.3	1.02
5	26883.7	26780.1	0.38
6	34334.7	34200.0	0.39
7	34926.2	34415.5	1.48
8	35768.9	35590.4	0.50

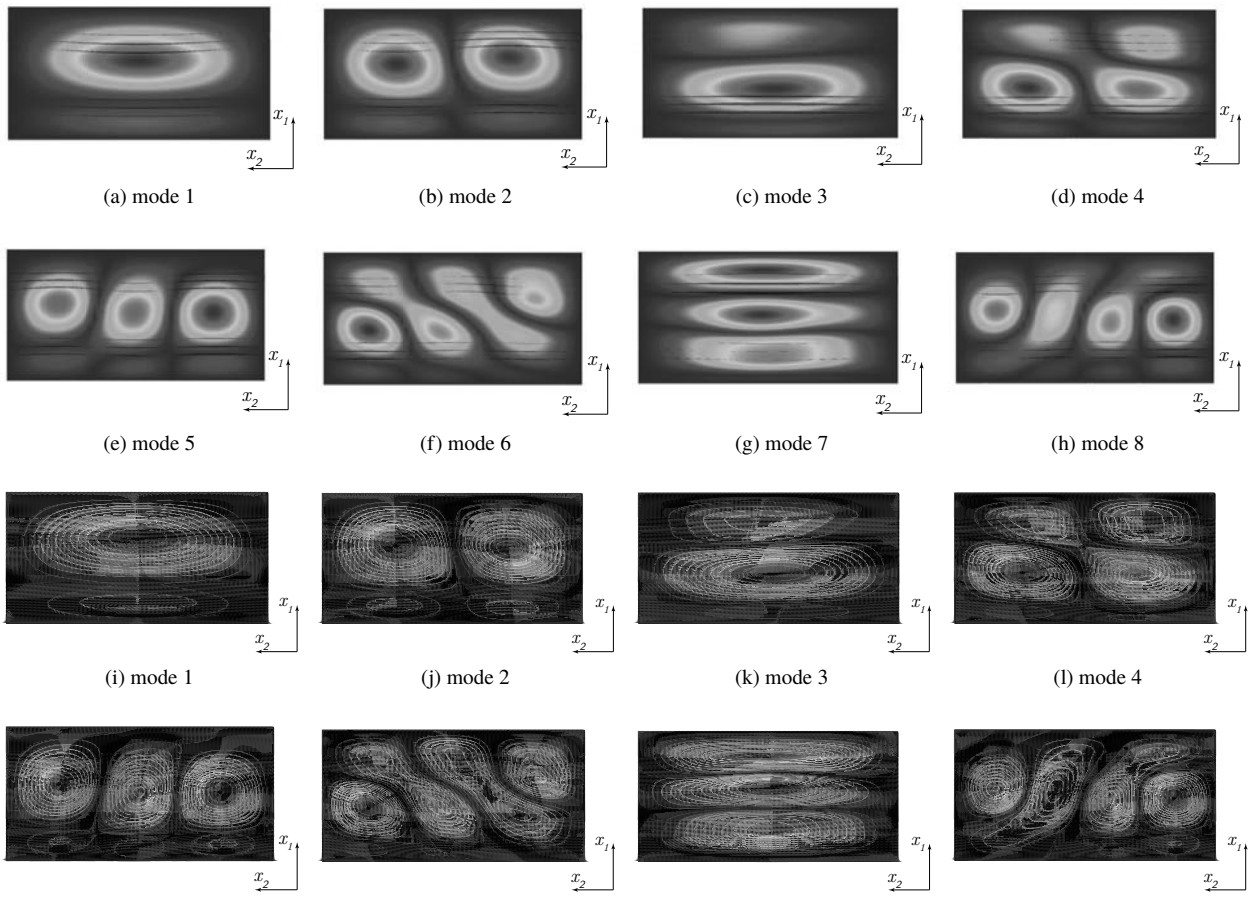

(a) mode 1 (b) mode 2 (c) mode 3 (d) mode 4

(e) mode 5 (f) mode 6 (g) mode 7 (h) mode 8

(i) mode 1 (j) mode 2 (k) mode 3 (l) mode 4

(m) mode 5 (n) mode 6 (o) mode 7 (p) mode 8

Figure 7 Natural mode shapes of vibration of a stiffened VS curved shell: present (Fig.7a to Fig.7h); FE (Fig.7i to Fig.7p);

width. A straight fiber layup is considered for the stiffeners, whose zero angle reference direction is taken along the x_2 direction. A ply thickness of $p_{th} = 0.25\,[mm]$ is considered and a detailed description of the layups is reported in Table 8. The material properties $CFRP_1$ are shown in Table 1. Symmetry restraints are imposed along the edges parallel to the x_2 direction and a clamped boundary condition is imposed along the edges parallel to the x_1 direction, as shown in Table 8. The analysis is conducted considering the entire structure subdivided in to nine shell domains ($R_D = 9$), following the same multi-domain scheme of $TC3$. For all domains $R_P = 10$ as it provides converged results. As for $TC3$, this multi-domain Ritz model has a total number of degrees of freedom $DOF_R = 5400$. To compare the results, an Abaqus finite element model with a converged mesh of 12800 $S4R$ elements is used. The FE has a total number of degrees of freedom $DOF_F = 78174$. The values of the first eight free vibration frequencies are shown in Table 9. Also reported is the relative difference with finite element results that is in any case smaller than 1.4%. The excellent agreement with FE results in also shown in Fig.9 where the corresponding mode shapes are presented along with FE results. Note that the proposed method requested a number of DOF_R that is less than 8% of the degrees of freedom required by FE, without any significant loss of accuracy and with a substantial reduction of computational time.
This last analysis completes the validation of the proposed approach for the free vibration of VS doubly curved stiffened shell structures.

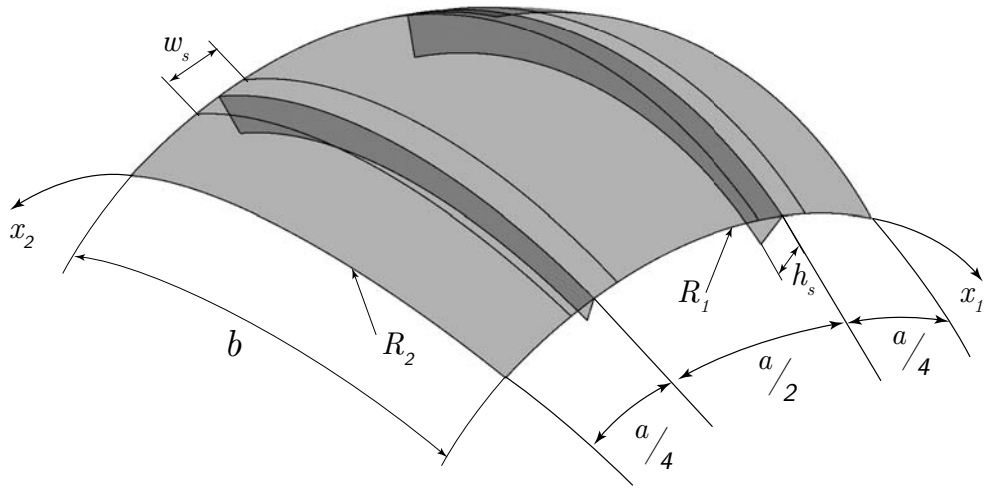

Figure 8 Geometry of a stiffened spherical shell

B. Transient analyses

To show the accuracy of the proposed method for the linear transient analyses of complex multi-part structures used in aerospace applications, original results for the dynamic response of the VS stiffened shell geometries discussed in Sec.V.A are considered. Different time dependant loading conditions are studied and the results are validated by comparison with finite element results.

Table 8 Geometry, layup and boundary conditions of a stiffened VS spherical shell.

Geometry:	$a = b = 0.4\,[m] \quad R_1 = R_2 = 0.4\,[m] \quad p_{th} = 0.25\,[mm]$
	$w_s = 0.05\,[m] \quad h_s = 0.03\,[m]$
Layup:	left shell $\left[\langle\langle 45\|90\rangle\rangle/\langle\langle -45\| -90\rangle\rangle/0_2\right]_s$
	central shell $\left[\langle 45\|90\rangle/\langle -45\| -90\rangle/0_2\right]_s$
	right shell $\left[\langle\langle 90\|45\rangle\rangle/\langle\langle -90\| -45\rangle\rangle/0_2\right]_s$
	stiffener flange $\left[\pm 90/0_4/\mp 90/\pm 45/90/0_2/90/\mp 45\right]$
	stiffener web $\left[\pm 45/90/0\right]_s$
BC:	$u_1 = \vartheta_2 = 0$ at $x_1 = \pm^a/_2$
	$u_1 = u_2 = u_3 = \vartheta_1 = \vartheta_2 = 0$ at $x_2 = \pm^b/_2$

Table 9 Natural frequencies [rad/s] of a VS stiffened spherical shell.

Mode	$R_P = 10$	FE	diff%
1	10998.3	11108.0	-0.98
2	11139.5	11229.9	-0.80
3	11325.2	11433.5	-0.94
4	11595.7	11755.8	-1.36
5	11773.0	11802.9	-0.25
6	12061.5	12207.6	-1.19
7	12339.8	12369.1	-0.23
8	12669.9	12791.3	-0.94

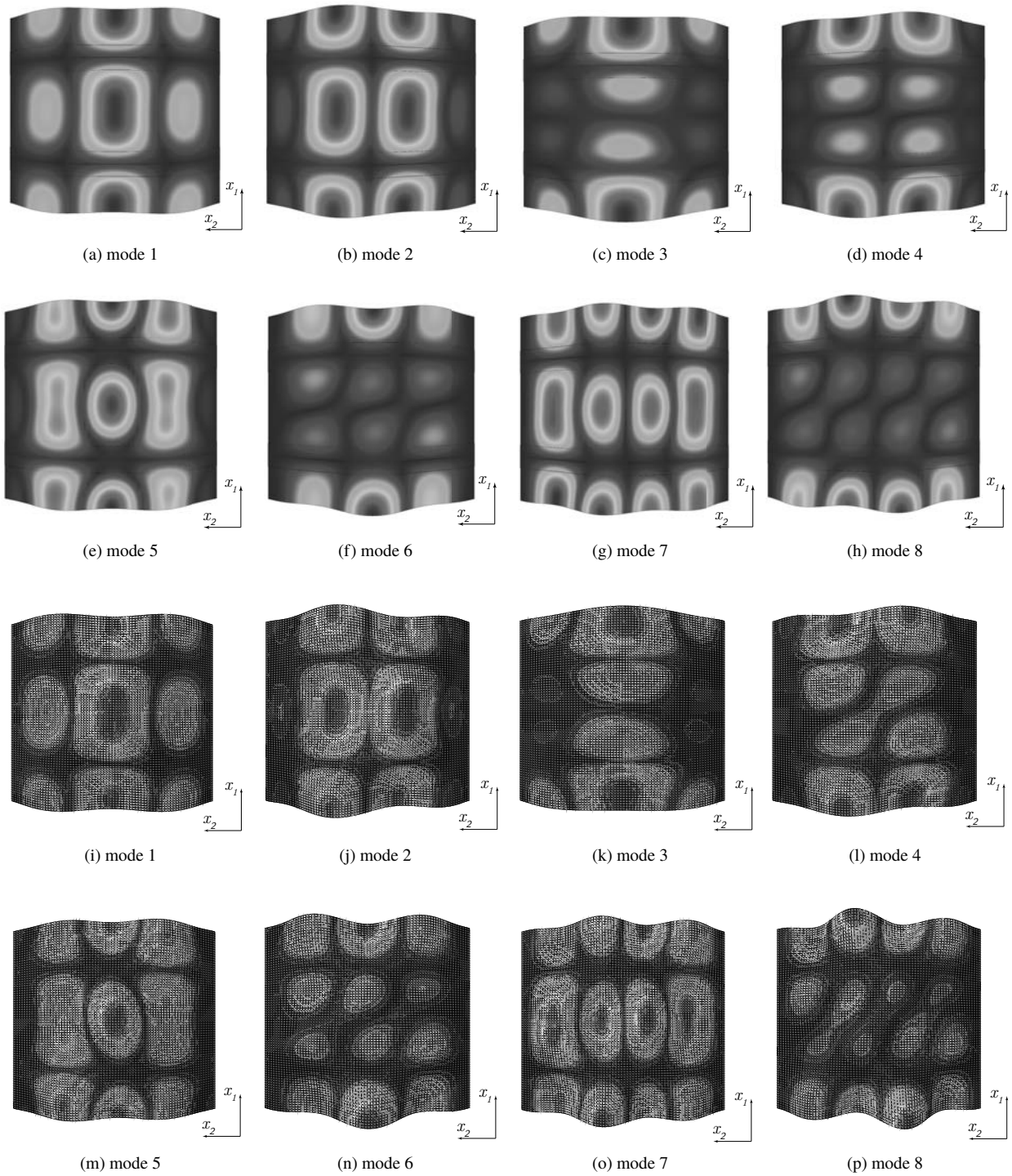

(a) mode 1 (b) mode 2 (c) mode 3 (d) mode 4

(e) mode 5 (f) mode 6 (g) mode 7 (h) mode 8

(i) mode 1 (j) mode 2 (k) mode 3 (l) mode 4

(m) mode 5 (n) mode 6 (o) mode 7 (p) mode 8

Figure 9 Natural mode shapes of vibration of a stiffened VS spherical shell: present (Fig.9a to Fig.9h); FE (Fig.9i to Fig.9p);

First, the variable curvature VS stiffened shell, $TC3$, shown in Fig.6 is considered. Details of geometry, layup and material are the same as in Sec.V.A and are detailed in Table 6 and Table 1. The shell structure is clamped on all of the outer edges and the analysis is conducted considering the entire structure to be subdivided in to nine shell domains ($R_D = 9$), following the same multi-domain scheme described in Sec.V.A. The structure is subjected to a uniform pressure load varying with time as $P(t) = 0.2 \sin(\omega_1 t) \quad [^N/_{mm^2}]$, where $\omega_1 = 12660.4\,[^{rad}/_s]$ is the fundamental circular frequency of the structure. All of the analyses are carried out by using a Newmark time integration scheme with a fixed time step $t_s = (^{5T_1}/_{400})$, where T_1 is the oscillation period of the fundamental frequency of the structure. The total analysis time is set equal to $5T_1$. In addition to the undamped case, two damped transient analyses are carried out by considering two different values for the damping coefficients ζ_2 and ζ_6 associated with the second and sixth natural frequencies, namely $\zeta_2 = \zeta_6 = \{0.01, 0.02\}$ (see Eqs.(44) and (45)). For all Ritz domains $R_P = 14$ is chosen as it provides converged results; this multi-domain Ritz model has a total number of degrees of freedom that is $DOF_R = 10584$. In order to verify the accuracy of the solution, Abaqus FE results are taken as reference and a finite element model with a mesh of 25600 $S4R$ elements is used for the analysis, resulting in a total number of degrees of freedom of $DOF_F = 155574$. This FE solution follow a convergence study that considered both $S4R$ and $S8R$ meshes and it is chosen as a reference as it gives the converged FE solution with the minimum number of degrees of freedom. A comparison of FE and Ritz results is shown in Fig.10 in terms of the time history of the vertical displacement of the midpoint of the shell in between the two stiffeners. The vertical displacement is normalised with respect to the shell thickness and the time in abscissa is normalised with respect to T_1. The structural response shown in Fig.10 is characterized by the typical resonance behaviour: exponentially growing amplitude related to the first natural mode of vibration. Indeed, setting the excitation frequency equal to the fundamental frequency is done in order to show the accuracy of the present approach for resonance analysis. Comparing the results shown in Figs.10a, 10b and 10c, the influence of increasing the damping factor is clearly displayed by the variation of the amplitude's extrema: higher damping factors lead to lower amplitudes in the dynamic response. Generally, the results show excellent agreement with FE results for all analyses, by using a number of DOF_R that is less than 7% of the degrees of freedom requested by the FE.

Referring to the VS stiffened spherical shell, $TC4$, shown in Fig.8, the linear transient response of the structure undergoing a step uniform pressure is studied. This particular loading condition leads to a complex time response of the structure resulting in a more computationally expensive analysis. This test case is specifically chosen to challenge further the present method. The considered geometry, layup and material are the same as in Sec.V.A and are detailed in Table 8 and Table 1. As described in Sec.V.A, symmetry restraints are imposed along the edges parallel to the x_2 direction and a clamped boundary condition is imposed along the edges parallel to the x_1 direction of the shell structure. The analysis is conducted considering that the entire structure is subdivided in to nine shell domains ($R_D = 9$) and for each of those $R_P = 22$ is used as this provides converged results; this multi-domain Ritz model counts a total number of

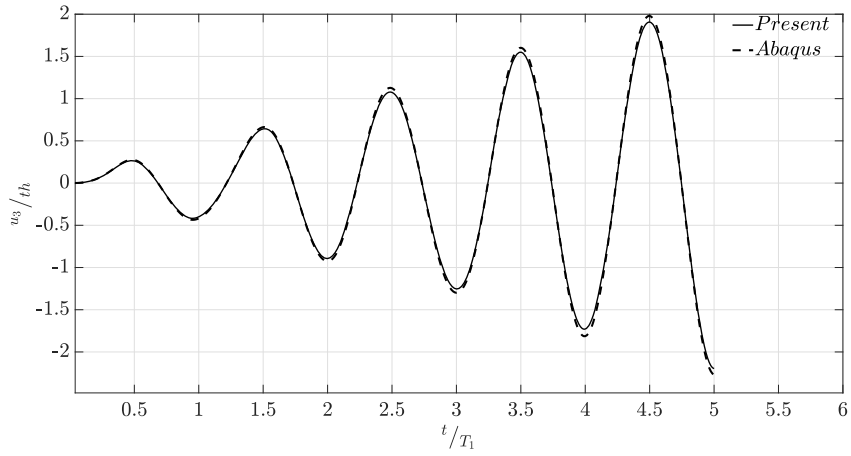

(a) $\zeta_2 = \zeta_6 = 0.0$

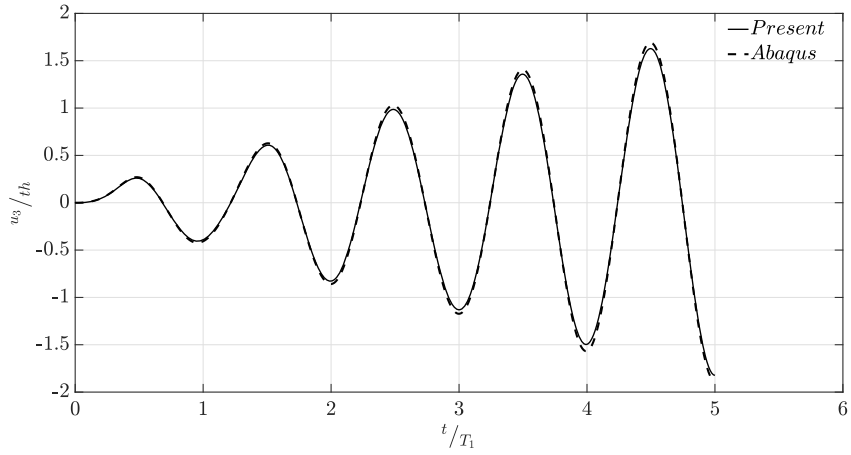

(b) $\zeta_2 = \zeta_6 = 0.01$

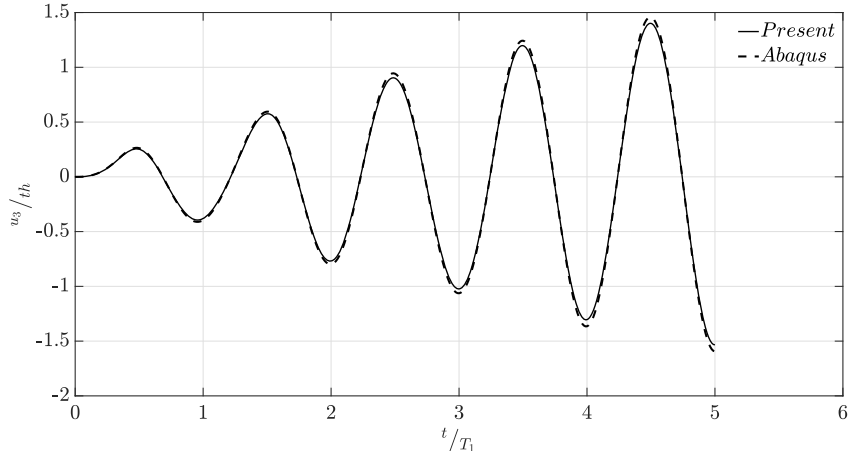

(c) $\zeta_2 = \zeta_6 = 0.02$

Figure 10 Stiffened VS variable curvature shell: time history of vertical displacement.

degrees of freedom that is $DOF_R = 26136$. The structure undergoes a uniform pressure step load $P(t) = 1.0 \quad [^N/_{mm^2}]$ for $t \geq 0$. In addition to the undamped response, the damped linear transient response has been studied by considering two different values for the damping coefficients ζ_2 and ζ_6 associated with the second and sixth natural frequencies, namely $\zeta_2 = \zeta_6 = \{0.01, 0.02\}$. To compare results, FE Abaqus solutions are considered. In particular a finite element model with a mesh of 12800 $S4R$ elements was used which has a total number of degrees of freedom $DOF_F = 78174$. Also in this case, this FE solution follows a convergence study that considered both $S4R$ and $S8R$ meshes and is used as a reference as it results in the converged FE solution with the minimum number of degrees of freedom. Both FE and Ritz analyses are carried out with a fixed time integration step $t_s = (^{5T_1}/_{400})$, where T_1 is the oscillation period of the fundamental frequency of the structure and the total analysis time is set equal to $5T_1$ in order to focus attention on the transient regime. The results are shown in Fig.11 in terms of the time history of the vertical displacement of the midpoint of the shell in between the two stiffeners. As shown in Fig.11, the dynamic structural behaviour is characterized by the contribution of different high frequency natural modes to the transient response of the structure. This behaviour was anticipated by the high density distribution of the natural modes of the structure in the frequency domain, as shown in Table 9 for the free vibration case study. Comparing the results shown in Figs.11a, 11b and 11c it is evident that increasing values of the damping factors leads to a reduction of the amplitudes of the response. This effect is more pronounced for the amplitudes of high frequency modes which, accordingly to the Rayleigh damping model herein adopted, suffer more dissipation. The converged Ritz solution is obtained using a number of DOF_R that is less than 34% of the degrees of freedom needed by the converged FE model and, as shown in Fig.11, the presented results show an excellent agreement with finite element solutions. However, despite the significant reduction of degrees of freedom needed for the analysis, the Ritz solution has a comparable computational time to that of Abaqus FE. In this regard, it is known that parameters like sparsity and bandwidth of the structural matrices play an important role for the overall computational time[51]. Hereof the numerical integration adopted determines the loss of any sort of sparsity of the structural matrices and increasing the number of R_D leads to the presence of off-diagonal blocks due to the penalty terms that enforce structural continuity. Note, if an issue, the bandwidth of the stiffness matrix could be reduced with an appropriate assembly and reordering strategy. Finally, it should be mentioned that the developed Ritz tool is not computationally optimized and that a faster tool could be obtained using more efficient programming languages (i.e. Fortran, C++) and using pre-compiled routines.

VI. Conclusion

In this work, a Ritz analysis method for free vibration and linear transient analysis of generally laminated, variable stiffness, doubly-curved shell structures is presented. Complex structural geometries are modeled as an assembly of shell-like domains. The doubly curved orthogonal shell kinematics is based on first-order shear deformation theory and no further assumption is made on the shallowness or on the thinness of the shell. The proposed formulation

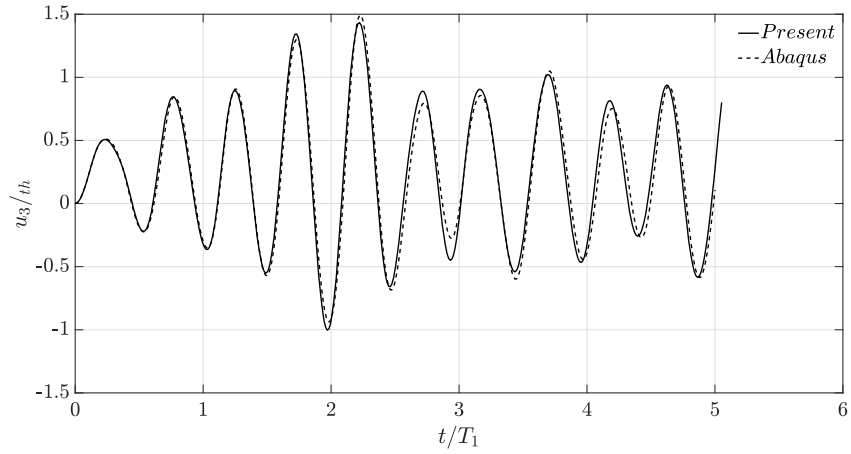

(a) $\zeta_2 = \zeta_6 = 0.0$

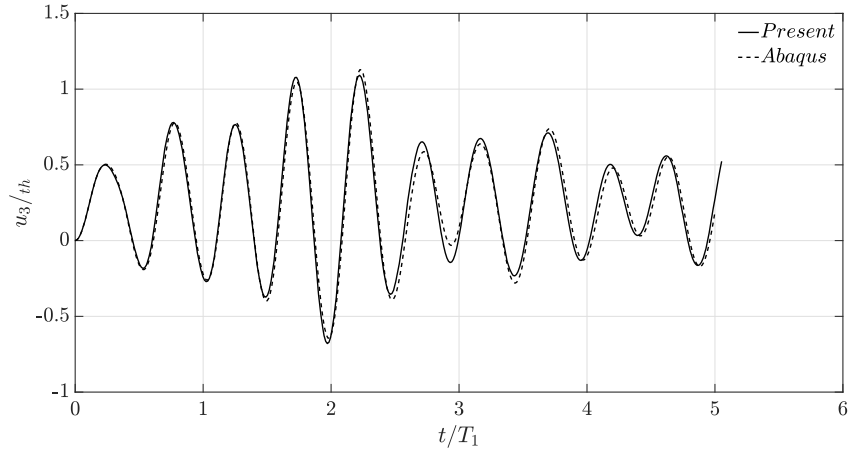

(b) $\zeta_2 = \zeta_6 = 0.01$

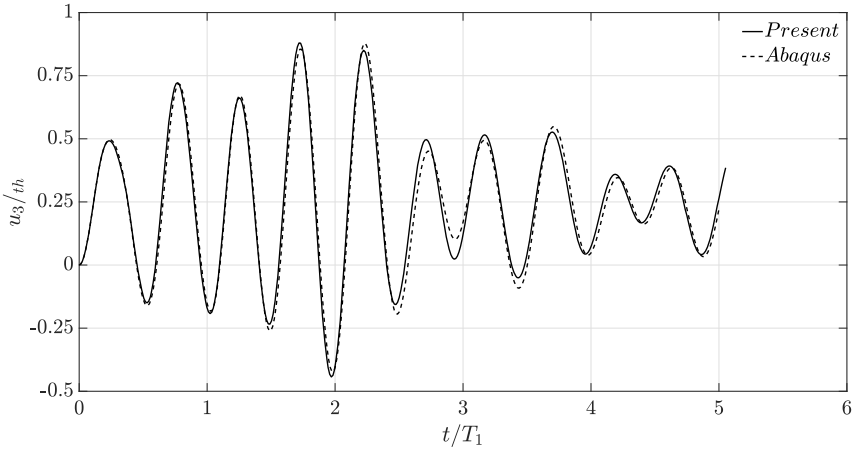

(c) $\zeta_2 = \zeta_6 = 0.02$

Figure 11 Stiffened VS spherical shell: time history of vertical displacement.

models general variable stiffness stacking sequences, arbitrary loads and boundary conditions. Furthermore, any geometrical approximation is introduced in the modeling technique by using a rational Bézier surface representation for the geometrical description of the shell structure. Following a Ritz discretization technique, Legendre orthogonal polynomials are employed to approximate the unknown displacement field and penalty techniques are used to enforce the displacements continuity of the assembled multi-domain structure and to apply the kinematical boundary conditions. For the linear transient solution, classical Rayleigh damping is considered and time integration is performed through the Newmark integration scheme. An analysis tool has been implemented that models a wide range of configurations and load cases for multi-component, variable stiffness composite structures, providing the same levels of accuracy as finite element analysis with a reduced number of variables and simplified data preparation. The efficiency and versatility of the analysis tool are shown along with original results for linear transient and free vibration analyses of variable stiffness, stiffened shell structures that, to the best of the authors' knowledge are presented here for the first time. The excellent properties of Legendre orthogonal polynomials for capturing local responses with few terms allow a significant reduction in the number of unknowns without any significant difference in the accuracy of the solution, when compared to finite elements procedures.

Acknowledgments

V. Oliveri and P.M. Weaver would like to thank Science Foundation Ireland for funding the Spatially and Temporally Variable Composite Structures grant no. (15/RP/2773) under its Research Professor program.

References

[1] Hyer, M., and Lee, H., "The use of curvilinear fiber format to improve buckling resistance of composite plates with central circular holes," *Composite Structures*, Vol. 18, 1991, pp. 239–261. doi:https://doi.org/10.1016/0263-8223(91)90035-W.

[2] Gürdal, Z., and Olmedo, R., "In-plane response of laminates with spatially varying fiber orientations-variable stiffness concept," *AIAA Journal*, Vol. 31, No. 4, 1993, pp. 751–758. doi:https://doi.org/10.2514/3.11613.

[3] Wu, Z., Raju, G., and Weaver, P. M., "Framework for the Buckling Optimization of Variable-Angle Tow Composite Plates," *AIAA Journal*, Vol. 53, No. 12, 2015, pp. 3788–3804. doi:https://doi.org/10.2514/1.J054029.

[4] Wu, Z., Weaver, P. M., Raju, G., and Kim, B. C., "Buckling analysis and optimisation of variable angle tow composite plates," *Thin-Walled Structures*, Vol. 60, 2012, pp. 163 – 172. doi:https://doi.org/10.1016/j.tws.2012.07.008.

[5] Ijsselmuiden, S. T., Abdalla, M. M., and Gürdal, Z., "Optimization of Variable-Stiffness Panels for Maximum Buckling Load Using Lamination Parameters," *AIAA Journal*, Vol. 48, No. 1, 2010, pp. 134–143. doi:https://doi.org/10.2514/1.42490.

[6] Zhao, W., and Kapania, R. K., "Prestressed Vibration of Stiffened Variable-Angle Tow Laminated Plates," *AIAA Journal*, 2019, pp. 1–19. doi:https://doi.org/10.2514/1.J057719.

[7] Ribeiro, P., and Akhavan, H., "Non-linear vibrations of variable stiffness composite laminated plates," *Composite Structures*, Vol. 94, 2012, pp. 2424–2432. doi:https://doi.org/10.1016/j.compstruct.2012.03.025.

[8] Akhavan, H., and Ribeiro, P., "Natural modes of vibration of variable stiffness composite laminates with curvilinear fibers," *Composite Structures*, Vol. 93, No. 11, 2011, pp. 3040 – 3047. doi:https://doi.org/10.1016/j.compstruct.2011.04.027.

[9] Yazdani, S., and Ribeiro, P., "A layerwise p-version finite element formulation for free vibration analysis of thick composite laminates with curvilinear fibres," *Composite Structures*, Vol. 120, 2015, pp. 531 – 542. doi:https://doi.org/10.1016/j.compstruct.2014.10.030.

[10] Akhavan, H., and Ribeiro, P., "Non-linear forced periodic oscillations of laminates with curved fibres by the shooting method," *International Journal of Non-Linear Mechanics*, Vol. 76, 2015, pp. 176 – 189. doi:https://doi.org/10.1016/j.ijnonlinmec.2015.06.004.

[11] Akhavan, H., and Ribeiro, P., "Geometrically non-linear periodic forced vibrations of imperfect laminates with curved fibres by the shooting method," *Composites Part B: Engineering*, Vol. 109, 2017, pp. 286 – 296. doi:https://doi.org/10.1016/j.compositesb.2016.10.059.

[12] Guenanou, A., and Houmat, A., "Free vibration analysis of symmetrically laminated composite circular plates with curvilinear fibers," *Science and Engineering of Composite Materials*, Vol. 24, No. 1, 2015, pp. 111–121. doi:https://doi.org/10.1515/secm-2014-0340.

[13] Houmat, A., "Three-dimensional free vibration analysis of variable stiffness laminated composite rectangular plates," *Composite Structures*, Vol. 194, 2018, pp. 398 – 412. doi:https://doi.org/10.1016/j.compstruct.2018.04.028.

[14] Samukham, S., Raju, G., Wu, Z., and Vyasarayani, C. P., "Dynamic instability analysis of variable angle tow composite plate with delamination around a cut-out," *Mechanics of Advanced Materials and Structures*, Vol. 26, No. 1, 2019, pp. 62–70. doi:https://doi.org/10.1080/15376494.2018.1534166.

[15] Vescovini, R., and Dozio, L., "A variable-kinematic model for variable stiffness plates: Vibration and buckling analysis," *Composite Structures*, Vol. 142, 2016, pp. 15 – 26. doi:https://doi.org/10.1016/j.compstruct.2016.01.068.

[16] Tan, P., and Nie, G., "Free and forced vibration of variable stiffness composite annular thin plates with elastically restrained edges," *Composite Structures*, Vol. 149, 2016, pp. 398 – 407. doi:https://doi.org/10.1016/j.compstruct.2016.04.021.

[17] Akbarzadeh, A., Nik, M. A., and Pasini, D., "Vibration responses and suppression of variable stiffness laminates with optimally steered fibers and magnetostrictive layers," *Composites Part B: Engineering*, Vol. 91, 2016, pp. 315 – 326. doi:https://doi.org/10.1016/j.compositesb.2016.02.003.

[18] Heydarpour, Y., and Aghdam, M., "A hybrid Bézier based multi-step method and differential quadrature for 3D transient response of variable stiffness composite plates," *Composite Structures*, Vol. 154, 2016, pp. 344 – 359. doi:https://doi.org/10.1016/j.compstruct.2016.07.060.

[19] Heydarpour, Y., and Aghdam, M., "A coupled integral-differential quadrature and B-spline-based multi-step technique for transient analysis of VSCL plates," *Acta Mechanica*, Vol. 228, No. 9, 2017, pp. 2965–2986. doi:https://doi.org/10.1007/s00707-017-1850-3.

[20] Lo, H.-C., and Hyer, M., "Fundamental Vibration Frequencies of Circular and Elliptical Composite Cylinders with Circumferentially Varying Fiber Orientation," *52nd AIAA/ASME/ASCE/AHS/ASC Structures, Structural Dynamics and Materials Conference*, 2011. doi:https://doi.org/10.2514/6.2011-1752.

[21] Ribeiro, P., "Non-linear modes of vibration of thin cylindrical shells in composite laminates with curvilinear fibres," *Composite Structures*, Vol. 122, 2015, pp. 184 – 197. doi:https://doi.org/10.1016/j.compstruct.2014.11.019.

[22] Ribeiro, P., and Stoykov, S., "Forced periodic vibrations of cylindrical shells in laminated composites with curvilinear fibres," *Composite Structures*, Vol. 131, 2015, pp. 462 – 478. doi:https://doi.org/10.1016/j.compstruct.2015.05.050.

[23] Wu, C.-P., and Lee, C.-Y., "Differential quadrature solution for the free vibration analysis of laminated conical shells with variable stiffness," *International Journal of Mechanical Sciences*, Vol. 43, No. 8, 2001, pp. 1853 – 1869. doi:https://doi.org/10.1016/S0020-7403(01)00010-8.

[24] Tornabene, F., Fantuzzi, N., Bacciocchi, M., and Viola, E., "Higher-order theories for the free vibrations of doubly-curved laminated panels with curvilinear reinforcing fibers by means of a local version of the GDQ method," *Composites Part B: Engineering*, Vol. 81, 2015, pp. 196 – 230. doi:https://doi.org/10.1016/j.compositesb.2015.07.012.

[25] Tornabene, F., Fantuzzi, N., and Bacciocchi, M., "Foam core composite sandwich plates and shells with variable stiffness: Effect of the curvilinear fiber path on the modal response," *Journal of Sandwich Structures & Materials*, 2017, pp. 1–46. doi:https://doi.org/10.1177/1099636217693623.

[26] Samukham, S., Raju, G., Vyasarayani, C., and Weaver, P. M., "Dynamic instability of curved variable angle tow composite panel under axial compression," *Thin-Walled Structures*, Vol. 138, 2019, pp. 302 – 312. doi:https://doi.org/10.1016/j.tws.2019.02.015.

[27] Venkatachari, A., Natarajan, S., and Ganapathi, M., "Variable stiffness laminated composite shells – Free vibration characteristics based on higher-order structural theory," *Composite Structures*, Vol. 188, 2018, pp. 407 – 414. doi:https://doi.org/10.1016/j.compstruct.2018.01.025.

[28] Oliveri, V., Milazzo, A., and Weaver, P., "Thermo-mechanical post-buckling analysis of variable angle tow composite plate assemblies," *Composite Structures*, Vol. 183, 2018, pp. 620 – 635. doi:https://doi.org/10.1016/j.compstruct.2017.07.050, in honor of Prof. Y. Narita.

[29] Milazzo, A., and Oliveri, V., "Buckling and Postbuckling of Stiffened Composite Panels with Cracks and Delaminations by Ritz Approach," *AIAA Journal*, 2016, pp. 1–16. doi:https://doi.org/10.2514/1.J055159.

[30] Gulizzi, V., Oliveri, V., and Milazzo, A., "Buckling and post-buckling analysis of cracked stiffened panels via an X-Ritz method," *Aerospace Science and Technology*, Vol. 86, 2019, pp. 268 – 282. doi:https://doi.org/10.1016/j.ast.2019.01.019.

[31] Chen, X., Nie, G., and Wu, Z., "Dynamic instability of variable angle tow composite plates with delamination," *Composite Structures*, Vol. 187, 2018, pp. 294 – 307. doi:https://doi.org/10.1016/j.compstruct.2017.12.042.

[32] Loja, M., Barbosa, J., and Soares, C. M., "Dynamic instability of variable stiffness composite plates," *Composite Structures*, Vol. 182, 2017, pp. 402 – 411. doi:https://doi.org/10.1016/j.compstruct.2017.09.046.

[33] Reddy, J., *Mechanics of laminated composite plates and shells. Theory and analysis*, CRC Press, 2004.

[34] Vescovini, R., and Bisagni, C., "Semi-analytical buckling analysis of omega stiffened panels under multi-axial loads," *Composite Structures*, Vol. 120, 2015, pp. 285 – 299. doi:https://doi.org/10.1016/j.compstruct.2014.10.003.

[35] Castro, S. G., and Donadon, M. V., "Assembly of semi-analytical models to address linear buckling and vibration of stiffened composite panels with debonding defect," *Composite Structures*, Vol. 160, 2017, pp. 232 – 247. doi:https://doi.org/10.1016/j.compstruct.2016.10.026.

[36] "7 - Stability of composite shell–type structures," *Stability and Vibrations of Thin Walled Composite Structures*, edited by H. Abramovich, Woodhead Publishing, 2017, pp. 253 – 428. doi:https://doi.org/10.1016/B978-0-08-100410-4.00007-7.

[37] Oliveira, B., Neto, E. L., and Monteiro, F., "An accurate Ritz approach for analysis of cracked stiffened plates," *Applied Mathematical Modelling*, Vol. 73, 2019, pp. 598 – 614. doi:https://doi.org/10.1016/j.apm.2019.04.014.

[38] Piegl, L., and Tiller, W., *The NURBS Book (2Nd Ed.)*, Springer-Verlag, Berlin, Heidelberg, 1997.

[39] Reddy, J., *Theory and analysis of elastic plates and shells.*, CRC Press, 2007.

[40] Hamilton, W. R., and Beaufort, F., "XV. On a general method in dynamics; by which the study of the motions of all free systems of attracting or repelling points is reduced to the search and differentiation of one central relation, or characteristic function," *Philosophical Transactions of the Royal Society of London*, Vol. 124, 1834, pp. 247–308. doi:https://doi.org/10.1098/rstl.1834.0017.

[41] Rayleigh, J. W. S., *The theory of sound*, New York, Dover, 1877.

[42] Kim, J., Dargush, G. F., and Ju, Y.-K., "Extended framework of Hamilton's principle for continuum dynamics," *International Journal of Solids and Structures*, Vol. 50, No. 20-21, 2013, pp. 3418–3429. doi:https://doi.org/10.1016/j.ijsolstr.2013.06.015.

[43] Zienkiewicz, O. C., and Taylor, R. L., *The Finite Element Method: Solid mechanics*, Butterworth-Heinemann, 2002.

[44] Bathe, K.-J., *Finite element procedures*, Klaus-Jurgen Bathe, 2006.

[45] Smith, S., Bradford, M., and Oehlers, D., "Numerical convergence of simple and orthogonal polynomials for the unilateral plate buckling problem using the Rayleigh-Ritz method," *International Journal for Numerical Methods in Engineering*, Vol. 44, No. 11, 1999, pp. 1685–1707. doi:https://doi.org/10.1002/(SICI)1097-0207(19990420)44:11<1685::AID-NME562>3.0.CO;2-9.

[46] Abramowitz, M., and Stegun, I. A., *Handbook of mathematical functions: with formulas, graphs, and mathematical tables*, Vol. 55, Courier Corporation, 1965.

[47] Yuan, J., and Dickinson, S., "Flexural vibration of rectangular plate systems approached by using artificial springs in the Rayleigh-Ritz method," *Journal of Sound and Vibration*, Vol. 159, No. 1, 1992, pp. 39–55. doi:https://doi.org/10.1016/0022-460X(92)90450-C.

[48] Milazzo, A., and Oliveri, V., "Post-buckling analysis of cracked multilayered composite plates by pb-2 Rayleigh-Ritz method," *Composite Structures*, Vol. 132, 2015, pp. 75–86. doi:https://doi.org/10.1016/j.compstruct.2015.05.007.

[49] "Chapter 9 - Numerical Integration," *Computational Methods in Engineering*, edited by S. Venkateshan and P. Swaminathan, Academic Press, Boston, 2014, pp. 317 – 373. doi:https://doi.org/10.1016/B978-0-12-416702-5.50009-0.

[50] Ribeiro, P., "Linear modes of vibration of cylindrical shells in composite laminates reinforced by curvilinear fibres." *Journal of Vibration and Control*, Vol. 22(20), 2016, pp. 4141–4158. doi:https://doi.org/10.1177/1077546315571661.

[51] Vescovini, R., Dozio, L., D'Ottavio, M., and Polit, O., "On the application of the Ritz method to free vibration and buckling analysis of highly anisotropic plates," *Composite Structures*, Vol. 192, 2018, pp. 460 – 474. doi:https://doi.org/10.1016/j.compstruct.2018.03.017.